Measurement of azimuthal hadron asymmetries in semi-inclusive deep inelastic scattering off unpolarised nucleons

C. Adolph [h], R. Akhunzyanov [g], M.G. Alexeev [ab], Yu. Alexandrov [o,20],
G.D. Alexeev [g], A. Amoroso [aa,ab], V. Andrieux [v], V. Anosov [g],
A. Austregesilo [j,q], B. Badełek [ae], F. Balestra [aa,ab], J. Barth [d], G. Baum [a],
R. Beck [c], Y. Bedfer [v], A. Berlin [b], J. Bernhard [m], R. Bertini [aa,ab],
K. Bicker [j,q], J. Bieling [d], R. Birsa [x], J. Bisplinghoff [c], M. Bodlak [s],
M. Boer [v], P. Bordalo [l,1], F. Bradamante [y,j], C. Braun [h], A. Bravar [x],
A. Bressan [y,x,*], M. Büchele [i], E. Burtin [v], L. Capozza [v], M. Chiosso [aa,ab],
S.U. Chung [q,2], A. Cicuttin [z,x], M.L. Crespo [z,x], Q. Curiel [v],
S. Dalla Torre [x], S.S. Dasgupta [f], S. Dasgupta [x], O.Yu. Denisov [ab],
S.V. Donskov [u], N. Doshita [ag], V. Duic [y], W. Dünnweber [p],
M. Dziewiecki [af], A. Efremov [g], C. Elia [y,x], P.D. Eversheim [c], W. Eyrich [h],
M. Faessler [p], A. Ferrero [v], A. Filin [u], M. Finger [s], M. Finger Jr. [s],
H. Fischer [i], C. Franco [l], N. du Fresne von Hohenesche [m,j],
J.M. Friedrich [q], V. Frolov [j], R. Garfagnini [aa,ab], F. Gautheron [b],
O.P. Gavrichtchouk [g], S. Gerassimov [o,q], R. Geyer [p], M. Giorgi [y,x],
I. Gnesi [aa,ab], B. Gobbo [x], S. Goertz [d], M. Gorzellik [i], S. Grabmüller [q],
A. Grasso [aa,ab], B. Grube [q], A. Guskov [g], T. Guthörl [i,3], F. Haas [q],
D. von Harrach [m], D. Hahne [d], R. Hashimoto [ag], F.H. Heinsius [i],
F. Herrmann [i], F. Hinterberger [c], Ch. Höppner [q], N. Horikawa [r,4],
N. d'Hose [v], S. Huber [q], S. Ishimoto [ag,5], A. Ivanov [g], Yu. Ivanshin [g],
T. Iwata [ag], R. Jahn [c], V. Jary [t], P. Jasinski [m], P. Joerg [i], R. Joosten [c],
E. Kabuß [m] D. Kang [m], B. Ketzer [q,6], G.V. Khaustov [u], Yu.A. Khokhlov [u,7],
Yu. Kisselev [g], F. Klein [d], K. Klimaszewski [ad], J.H. Koivuniemi [b],
V.N. Kolosov [u], K. Kondo [ag], K. Königsmann [i], I. Konorov [o,q],

V.F. Konstantinov [u], A.M. Kotzinian [aa,ab], O. Kouznetsov [g], Z. Kral [t], M. Krämer [q], Z.V. Kroumchtein [g], N. Kuchinski [g], F. Kunne [v,*], K. Kurek [ad], R.P. Kurjata [af], A.A. Lednev [u], A. Lehmann [h], S. Levorato [x], J. Lichtenstadt [w], A. Maggiora [ab], A. Magnon [v], N. Makke [y,x,8], G.K. Mallot [j], C. Marchand [v], A. Martin [y,x], J. Marzec [af], J. Matousek [s], H. Matsuda [ag], T. Matsuda [n], G. Meshcheryakov [g], W. Meyer [b], T. Michigami [ag], Yu.V. Mikhailov [u], Y. Miyachi [ag], A. Nagaytsev [g], T. Nagel [q], F. Nerling [m], S. Neubert [q], D. Neyret [v], V.I. Nikolaenko [u], J. Novy [t], W.-D. Nowak [i], A.S. Nunes [l], I. Orlov [g], A.G. Olshevsky [g], M. Ostrick [m], R. Panknin [d], D. Panzieri [ac,ab], B. Parsamyan [aa,ab], S. Paul [q], M. Pesek [s], D. Peshekhonov [g], G. Piragino [aa,ab], S. Platchkov [v], J. Pochodzalla [m], J. Polak [k,x], V.A. Polyakov [u], J. Pretz [d,9], M. Quaresma [l], C. Quintans [l], S. Ramos [l,1], G. Reicherz [b], E. Rocco [j], V. Rodionov [g], E. Rondio [ad], A. Rychter [af], N.S. Rossiyskaya [g], D.I. Ryabchikov [u], V.D. Samoylenko [u], A. Sandacz [ad], S. Sarkar [f], I.A. Savin [g], G. Sbrizzai [y,x,*], P. Schiavon [y,x], C. Schill [i], T. Schlüter [p], A. Schmidt [h], K. Schmidt [i,3], H. Schmieden [d], K. Schönning [j], S. Schopferer [i], M. Schott [j], O.Yu. Shevchenko [g], L. Silva [l], L. Sinha [f], S. Sirtl [i], M. Slunecka [g], S. Sosio [aa,ab], F. Sozzi [x], A. Srnka [e], L. Steiger [x], M. Stolarski [l], M. Sulc [k], R. Sulej [ad], H. Suzuki [ag,4], A. Szableski [ad], T. Szameitat [i], P. Sznajder [ad], S. Takekawa [ab], J. ter Wolbeek [i,3], S. Tessaro [x], F. Tessarotto [x], F. Thibaud [v], S. Uhl [q], I. Uman [p], M. Vandenbroucke [v], M. Virius [t], J. Vondra [t], L. Wang [b], T. Weisrock [m], M. Wilfert [m], R. Windmolders [d], W. Wiślicki [ad], H. Wollny [v], K. Zaremba [af], M. Zavertyaev [o], E. Zemlyanichkina [g], M. Ziembicki [af]

[a] *Universität Bielefeld, Fakultät für Physik, 33501 Bielefeld, Germany* [10]
[b] *Universität Bochum, Institut für Experimentalphysik, 44780 Bochum, Germany* [10,17]
[c] *Universität Bonn, Helmholtz-Institut für Strahlen- und Kernphysik, 53115 Bonn, Germany* [10]
[d] *Universität Bonn, Physikalisches Institut, 53115 Bonn, Germany* [10]
[e] *Institute of Scientific Instruments, AS CR, 61264 Brno, Czech Republic* [11]
[f] *Matrivani Institute of Experimental Research & Education, Calcutta-700 030, India* [12]
[g] *Joint Institute for Nuclear Research, 141980 Dubna, Moscow Region, Russia* [13]
[h] *Universität Erlangen–Nürnberg, Physikalisches Institut, 91054 Erlangen, Germany* [10]
[i] *Universität Freiburg, Physikalisches Institut, 79104 Freiburg, Germany* [10,17]
[j] *CERN, 1211 Geneva 23, Switzerland*
[k] *Technical University in Liberec, 46117 Liberec, Czech Republic* [11]
[l] *LIP, 1000-149 Lisbon, Portugal* [14]
[m] *Universität Mainz, Institut für Kernphysik, 55099 Mainz, Germany* [10]
[n] *University of Miyazaki, Miyazaki 889-2192, Japan* [15]
[o] *Lebedev Physical Institute, 119991 Moscow, Russia*

[p] *Ludwig-Maximilians-Universität München, Department für Physik, 80799 Munich, Germany* [10,16]

[q] *Technische Universität München, Physik Department, 85748 Garching, Germany* [10,16]

[r] *Nagoya University, 464 Nagoya, Japan* [15]

[s] *Charles University in Prague, Faculty of Mathematics and Physics, 18000 Prague, Czech Republic* [11]

[t] *Czech Technical University in Prague, 16636 Prague, Czech Republic* [11]

[u] *State Research Center of the Russian Federation, Institute for High Energy Physics, 142281 Protvino, Russia*

[v] *CEA IRFU/SPhN Saclay, 91191 Gif-sur-Yvette, France* [17]

[w] *Tel Aviv University, School of Physics and Astronomy, 69978 Tel Aviv, Israel* [18]

[x] *Trieste Section of INFN, 34127 Trieste, Italy*

[y] *University of Trieste, Department of Physics, 34127 Trieste, Italy*

[z] *Abdus Salam ICTP, 34151 Trieste, Italy*

[aa] *University of Turin, Department of Physics, 10125 Turin, Italy*

[ab] *Torino Section of INFN, 10125 Turin, Italy*

[ac] *University of Eastern Piedmont, 15100 Alessandria, Italy*

[ad] *National Centre for Nuclear Research, 00-681 Warsaw, Poland* [19]

[ae] *University of Warsaw, Faculty of Physics, 00-681 Warsaw, Poland* [19]

[af] *Warsaw University of Technology, Institute of Radioelectronics, 00-665 Warsaw, Poland* [19]

[ag] *Yamagata University, Yamagata, 992-8510, Japan* [15]

[*] Corresponding authors.

E-mail addresses: Andrea.Bressan@cern.ch (A. Bressan), Fabienne.Kunne@cern.ch (F. Kunne), Giulio.Sbrizzai@ts.infn.it (G. Sbrizzai).

Abstract

Spin-averaged asymmetries in the azimuthal distributions of positive and negative hadrons produced in deep inelastic scattering were measured using the CERN SPS longitudinally polarised muon beam at 160 GeV/c and a ^{6}LiD target. The amplitudes of the three azimuthal modulations $\cos\phi_h$, $\cos 2\phi_h$ and $\sin\phi_h$ were obtained binning the data separately in each of the relevant kinematic variables x, z or p_T^h and binning in a three-dimensional grid of these three variables. The amplitudes of the $\cos\phi_h$ and $\cos 2\phi_h$ modulations show strong kinematic dependencies both for positive and negative hadrons.

© 2014 CERN for the benefit of the COMPASS Collaboration. Published by Elsevier B.V. This is an open access article under the CC BY license (http://creativecommons.org/licenses/by/3.0/). Funded by SCOAP^3.

1. Introduction

In the quark–parton model the transverse degrees of freedom of the nucleon constituents are usually integrated over, and the parton distribution functions (PDFs) as determined in lepton–nucleon deep inelastic scattering (DIS) depend only on the Bjorken scaling variable x and on Q^2, the virtuality of the exchanged photon. On the other hand it was soon realised [1,2] that in semi-inclusive DIS processes, namely in lepton–nucleon DIS in which at least one hadron from the current jet is detected, a possible intrinsic transverse momentum of the target quark would cause measurable effects in the cross-section. Indeed the semi-inclusive DIS cross-section is expected to exhibit a $\cos\phi_h$ and a $\cos 2\phi_h$ modulation, where ϕ_h is the angle between the lepton scattering plane and the plane defined by the hadron and the virtual photon directions, as shown in Fig. 1. The coefficients of these modulations are predicted to vanish asymptotically as $1/Q$ and $1/Q^2$, respectively [2]. The early measurements in the 70s however were not accurate enough to detect such modulations.

At the end of the 70s, interest in possible modulations of the semi-inclusive DIS cross-section came also from a different direction. Azimuthal asymmetries in unpolarised processes in quantum chromodynamics (QCD) are generated by gluon radiation and splitting, and the observation of these asymmetries was in fact proposed as a test of perturbative QCD (pQCD) [3]. Such a possibility however was immediately questioned by R. Cahn [4]. Using simple kinematics the amplitudes of the azimuthal modulations expected from the quark intrinsic transverse momentum could be computed and shown to be the dominant term as long as both Q^2 and the hadron transverse momentum are not too large [4]. Azimuthal modulations in the semi-inclusive DIS cross-section were indeed first observed by the EMC Collaboration [5,6] and then at FNAL [7], and at higher energies by the ZEUS experiment at HERA [8]. The present understanding is that
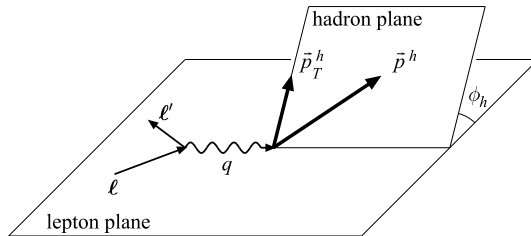

Fig. 1. Semi-inclusive DIS in the $\gamma^* N$ system: $\vec{p}^{\,h}$ is the momentum of the produced hadron and $\vec{p}_T^{\,h}$ its transverse component with respect to the virtual photon direction.

pQCD accounts for the asymmetries at large values of the final-state hadron transverse momentum p_T^h, while at low values ($p_T^h \lesssim 1$ GeV/c) it is the intrinsic transverse motion of the quarks which plays the key role [9].

Intrinsic transverse momentum has recently attracted much attention in connection with the great experimental and theoretical effort to understand the origin of the nucleon spin and, in particular, the many transverse spin effects in hadronic reactions observed since several decades. The PDFs of the nucleon have been generalised to include this new degree of freedom, introducing the transverse-momentum-dependent (TMD) distributions. Also, TMD fragmentation functions (FF) have been introduced, the best known being the Collins FF, which describes a correlation between the transverse momentum $\vec{p}_T^h$ of each of the hadrons in a hadronic jet and the spin of the fragmenting quark in the hadronisation process of a transversely polarised quark. The knowledge of this new sector of hadronic physics is still at its beginning, but several new important phenomena have been assessed [10] within a solid theoretical QCD framework [11]. Within this framework, much attention has been payed to distributions which are T-odd and for a long time were believed to be zero to preserve T-invariance. It was demonstrated afterwards that either initial or final state interactions can result in non-zero T-odd distributions. One T-odd PDF, the Sivers function, has already been shown to be definitely different from zero in semi-inclusive DIS processes off transversely polarised protons, even at high energies [12,13]. Another T-odd TMD PDF is the so-called Boer–Mulders function, which describes the correlation between the quark transverse spin and its transverse momentum in an unpolarised nucleon [14]. On top of the Cahn effect, the Boer–Mulders TMD PDF convoluted with the Collins FF is expected to contribute to the amplitudes of the $\cos\phi_h$ and $\cos 2\phi_h$ modulations in unpolarised semi-inclusive DIS processes and its extraction from the cross-section data is an important goal of the more recent investigations at lower energies by the HERMES Collaboration [15] and by the CLAS Collaboration [16].

In this paper, first results on the azimuthal modulations in unpolarised semi-inclusive DIS obtained by the COMPASS experiment are presented. The paper is organised as follows. Section 2 summarises the formalism for the semi-inclusive DIS cross-section in the one-photon exchange approximation. A short description of the experimental apparatus during the 2004 run is given in Section 3. The data analysis, the method used to extract the azimuthal asymmetries and the studies of the possible systematic effects are described in Sections 4, 5 and 6. Finally, the results are given in Section 7.

2. The semi-inclusive DIS cross-section

The spin-averaged differential semi-inclusive DIS cross-section for the production of a hadron h with transverse momentum p_T^h and a fraction z of the available energy is given in the one-photon exchange approximation [17] by:

$$\frac{d\sigma}{p_T^h \, dp_T^h \, dx \, dy \, dz \, d\phi_h} = \sigma_0 \big(1 + \epsilon_1 A_{\cos\phi_h}^{UU} \cos\phi_h$$
$$+ \epsilon_2 A_{\cos 2\phi_h}^{UU} \cos 2\phi_h + \lambda \epsilon_3 A_{\sin\phi_h}^{LU} \sin\phi_h \big), \tag{1}$$

where σ_0 is the ϕ_h independent part of the cross-section, λ is the longitudinal polarisation of the incident lepton, y is the fractional energy of the virtual photon, and the quantities ϵ_i are given by:

$$\epsilon_1 = \frac{2(2-y)\sqrt{1-y}}{1+(1-y)^2}, \qquad \epsilon_2 = \frac{2(1-y)}{1+(1-y)^2}, \qquad \epsilon_3 = \frac{2y\sqrt{1-y}}{1+(1-y)^2}. \tag{2}$$

The amplitudes $A^{XU}_{f(\phi_h)}$ will be referred to as azimuthal asymmetries in the following. The superscripts UU and LU refer to unpolarised beam and target, and to longitudinally polarised beam and unpolarised target, respectively.

The $\cos \phi_h$ and the $\cos 2\phi_h$ asymmetries are related to the Cahn effect and to the Boer–Mulders TMD PDF. The Cahn effect contributions to $A^{UU}_{\cos \phi_h}$ and $A^{UU}_{\cos 2\phi_h}$ originate from kinematics, when the intrinsic transverse momenta $\vec{k}_T$ of quarks inside the nucleon is taken into account, starting from the elastic quark–lepton cross-section [4]. Also the Boer–Mulders function contributes to both $A^{UU}_{\cos \phi_h}$ and $A^{UU}_{\cos 2\phi_h}$, where it appears convoluted with the Collins FF. The $A^{LU}_{\sin \phi_h}$ asymmetry is due to higher-twist effects and has no clear interpretation in terms of the parton model.

The amplitudes of the $\cos \phi_h$ and $\cos 2\phi_h$ modulations have been measured in semi-inclusive DIS on unpolarised proton and deuteron targets in a kinematic region similar to that of COMPASS by previous experiments [5,7] and at higher energies by the ZEUS experiment [8]. Results at lower energies have been recently published by HERMES [15] for positive and negative hadrons separately and by CLAS [16] for π^+.

COMPASS has presented preliminary results for $A^{UU}_{\cos \phi_h}$, $A^{UU}_{\cos 2\phi_h}$ and $A^{LU}_{\sin \phi_h}$ on the deuteron for positive and negative hadrons in 2008 [18]. A more refined analysis on a limited phase space as well as the removal of some specific problems related to the acceptance correction has lead to the final results presented here. They have been obtained from the data collected in 2004 with the transversely polarised ^{6}LiD target to measure the Collins and Sivers asymmetries [19].

3. The experimental apparatus

A brief description of the 2004 COMPASS apparatus is given in this section. More details on the COMPASS spectrometer can be found in Ref. [20].

The μ^+ beam was naturally polarised by the π decay mechanism, and the beam polarisation λ was about -80%. The beam intensity was $2 \cdot 10^8$ μ^+ per spill of 4.8 s with a cycle time of 16.8 s. The μ^+ momentum (~ 160 GeV/c) was measured event by event in a Beam Momentum Station (BMS) with a precision $\Delta p/p \lesssim 1\%$.

As the study of the nucleon spin was the main purpose of the experiment, a polarised target system was used in 2004. It consisted of two cells, each 60 cm long, filled with ^{6}LiD, placed on the beam line, and housed in a cryostat positioned along the axis of a solenoidal magnet. The ^{6}LiD grains were immersed in a mixture of liquid ^{3}He/^{4}He. A small contamination of ^{7}Li almost exactly balances the proton excess in ^{3}He, so that the target can effectively be regarded to be isoscalar. The data used in the present analysis (25% of the full 2004 data sample) have been taken with the target transversely polarised, i.e. polarised along the direction of the dipole field (0.42 T) provided by two additional saddle coils. The two target cells were oppositely polarised, so data were taken simultaneously for the two target polarisation states. In order to keep systematic effects under control, the orientation of the polarisation was reversed every 4 to 5 days (referred to as a "period" of data taking in the following).

The spectrometer consists of two magnetic stages and comprises a variety of tracking detectors, a RICH detector, two hadron calorimeters, and thick absorbers providing muon identification. The first stage is centred around the spectrometer magnet SM1, located 4 m downstream from the target centre, which has a bending power of 1 Tm and a large opening angle to contain the hadrons of the current jet. The second stage uses the spectrometer magnet SM2 (operated

at a bending power of 4.4 Tm), located 18 m downstream from the target, with an acceptance of ± 50 and ± 25 mrad in the horizontal and vertical planes, respectively. In order to match the expected particle flux at various locations along the spectrometer, various tracking detectors are used. The small-area trackers consist of several stations of scintillating fibres, silicon detectors, micromegas chambers and gaseous chambers using the GEM technique. Large-area tracking devices are made from gaseous detectors (Drift Chambers, Straw Tubes, and MWPC's) placed around the two spectrometer magnets.

Muons are identified in large-area detectors using drift-tubes downstream of iron or concrete absorbers. Hadrons are detected by two large iron-scintillator sampling calorimeters, installed in front of the absorbers and shielded to avoid electromagnetic contamination. The charged particle identification relies on the RICH technology, but is not used in this analysis where results are given for non-identified charged hadrons only.

In most DIS events the scattered muon is identified by coincidence signals in the trigger hodoscopes which measure the particle trajectory in the vertical (non-bending) plane and check its compatibility with the target position. Several veto counters upstream of the target are used to avoid triggers due to beam halo muons. In addition to this inclusive trigger mode, several semi-inclusive triggers select events fulfilling requirements based on the muon energy loss and on the presence of a hadron signal in the calorimeters. The acceptance is further extended toward high Q^2 values by the addition of a standalone calorimetric trigger in which no condition is set for the scattered muon.

4. Event selection and kinematic distributions

The DIS event and hadron selections are performed as in previous analyses based on the same data [19], and only a short description of the procedure is given here.

A track reconstructed in the scintillating fibres and silicon detectors upstream of the target is assumed to be an incoming muon if its momentum is measured in the BMS. Scattered muons are selected among the positively charged outgoing tracks with a momentum larger than 1 GeV/c, passing through SM1. In order to be accepted as the scattered muon, a track is required to cross an amount of material in the spectrometer corresponding to at least 30 radiation lengths and must be compatible with the hits in the trigger hodoscopes. Only events with one scattered muon candidate are accepted. The muon interaction point (the so-called "primary vertex") is defined by one beam particle and the scattered muon. The DIS events are selected requiring $Q^2 > 1$ (GeV/c)^2, $0.1 < y < 0.9$, and an invariant mass of the hadronic final state system $W > 5$ GeV/c^2.

If the amount of material traversed in the spectrometer is less than 10 radiation lengths the outgoing particles are assumed to be hadrons. In order to have a good resolution on the azimuthal angle the charged hadrons are required to have at least 0.1 GeV/c transverse momentum p_T^h with respect to the virtual photon direction. In order to reject hadrons from target fragmentation the hadrons are also required to carry a fraction $z > 0.2$ of the available energy while the contamination from hadrons produced in exclusive reactions is reduced by requiring z to be smaller than 0.85. No attempt is made to further suppress diffractive meson production, as done e.g. in Ref. [15].

In addition to these standard requirements, further cuts have been applied specific for this analysis because it requires acceptance corrected azimuthal distributions of the final state hadrons. An upper limit on the transverse hadron momentum has been introduced ($p_T^h < 1.0$ GeV/c), both to ensure negligible pQCD corrections and to obtain a better determined hadron acceptance. In

Table 1
Final statistics used for the azimuthal asymmetry evaluation for each of the 4 data-taking periods.

Period	Positive hadrons	Negative hadrons	Polarisation
1	$3.9 \cdot 10^5$	$3.4 \cdot 10^5$	$+$
2	$3.4 \cdot 10^5$	$2.9 \cdot 10^5$	$-$
3	$5.8 \cdot 10^5$	$5.0 \cdot 10^5$	$+$
4	$3.6 \cdot 10^5$	$3.1 \cdot 10^5$	$-$

order to have a flat azimuthal acceptance the cut $\theta_{\gamma^*}^{lab} < 60$ mrad is applied, where $\theta_{\gamma^*}^{lab}$ is the virtual photon polar angle calculated with respect to the nominal beam direction in the laboratory system. The cuts $y > 0.2$ and $x < 0.13$ have been also applied because of the correlation of x and y with $\theta_{\gamma^*}^{lab}$.

The final event and hadron selection is thus:

$$Q^2 > 1 \ (\text{GeV}/c)^2, \ W > 5 \ \text{GeV}/c^2, \ 0.003 < x < 0.13, \ 0.2 < y < 0.9,$$
$$\theta_{\gamma^*}^{lab} < 60 \ \text{mrad}, \ 0.2 < z < 0.85 \ \text{and} \ 0.1 \ \text{GeV}/c < p_T^h < 1.0 \ \text{GeV}/c.$$

The statistics of the hadron sample after all cuts is given in Table 1 for each of the 4 periods of data taken with the transversely polarised ^{6}LiD target in 2004. The data with opposite polarisation have been combined after normalising them on the relative incoming muon flux. The hadron standard sample consists mainly of pions [21], about 70% for positive hadrons, 76% in case of negative hadrons. Positive kaons and protons amount to about 15% each, negative kaons and antiprotons amount to 16% and 8%, respectively, as evaluated with a LEPTO Monte Carlo and cross-checked with the RICH detector.

The x distribution and the Q^2 distribution for the final sample are shown in Fig. 2 together with the hadron p_T^h and z distributions. The mean values of y and Q^2 with respect to x, z, and p_T^h are shown in Fig. 3.

5. Extraction of the azimuthal asymmetries

5.1. The method

From Eq. (1), the measured azimuthal distributions are expected to be:

$$N(\phi_h, \vec{v}) = N_0(\vec{v}) a(\phi_h, \vec{v}) \big[1 + \epsilon_1 A_{\cos \phi_h}^{UU}(\vec{v}) \cos \phi_h$$
$$+ \epsilon_2 A_{\cos 2\phi_h}^{UU}(\vec{v}) \cos 2\phi_h + \epsilon_3 \lambda A_{\sin \phi_h}^{LU}(\vec{v}) \sin \phi_h \big], \tag{3}$$

where $a(\phi_h, \vec{v})$ is the apparatus acceptance and $\vec{v}$ indicates the generic set of kinematic variables $(x, z, p_T^h, \dots)$ on which the apparatus acceptance and the azimuthal asymmetries can depend. In order to extract the azimuthal asymmetries it is necessary to correct the measured azimuthal distributions by the ϕ_h dependent part of the apparatus acceptance and to fit the corrected distribution with the appropriate ϕ_h modulation.

The azimuthal asymmetries have been first extracted from the data binned in x, z or p_T^h, and integrated over the other two variables ("integrated asymmetries"). The bin widths have been chosen to be larger than the experimental resolution estimated from Monte Carlo simulations. In each kinematic bin the azimuthal distributions $N(\phi_h)$ are produced separately for positive and negative hadrons, dividing the $(0, 2\pi)$ ϕ_h range into 16 bins. The apparatus acceptance $a(\phi_h)$ is
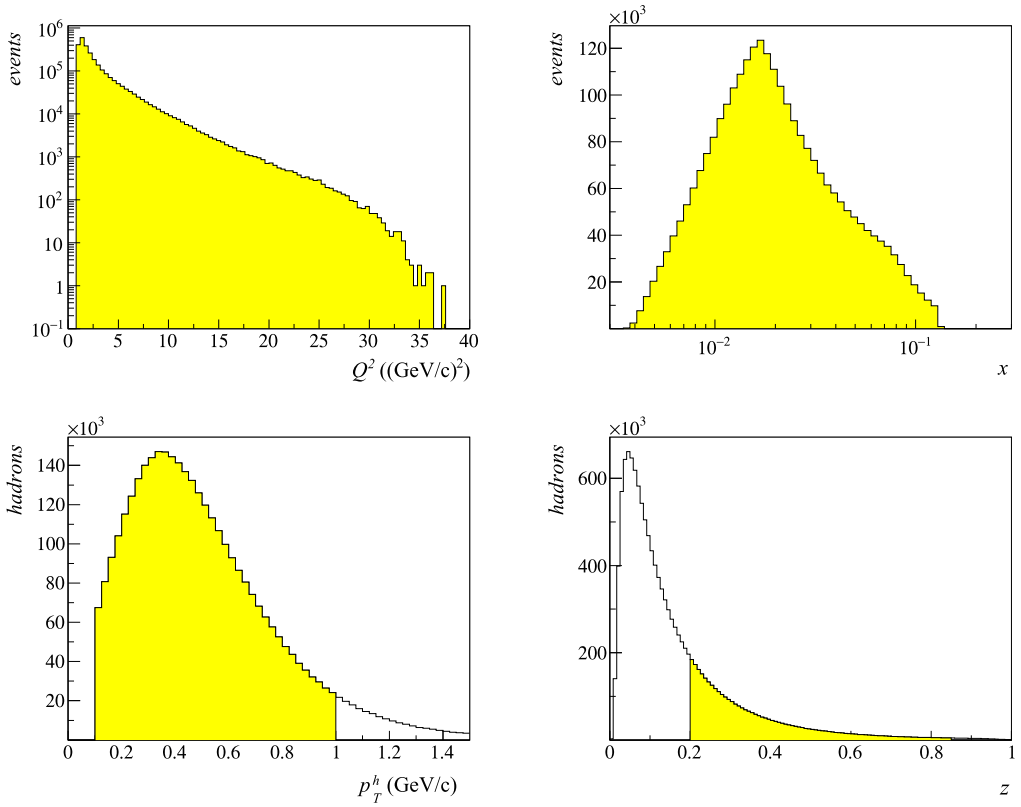
Fig. 2. Upper row: Q^2 and x distributions of all the events in the final sample. Lower row: p_T^h and z hadron distributions for the same sample of events.
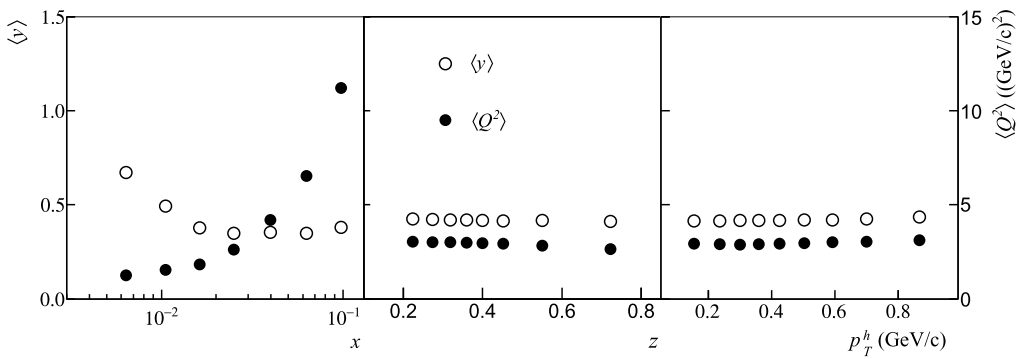
Fig. 3. Q^2 and y mean values calculated in the bins of x, of z and of p_T^h.

calculated from Monte Carlo simulations for positive and negative hadrons for each bin of ϕ_h and for each kinematic bin, as will be described in Section 5.2. The hadron azimuthal distributions corrected for the apparatus acceptance $N_{corr}(\phi_h) = N(\phi_h)/a(\phi_h)$ are then fitted with a four parameter function: $F(\phi_h) = p_0 \cdot (1 + p_{\cos\phi_h} \cdot \cos\phi_h + p_{\cos 2\phi_h} \cdot \cos 2\phi_h + p_{\sin\phi_h} \cdot \sin\phi_h)$. The

azimuthal asymmetries are then obtained by dividing the fitted parameters by the appropriate quantities, i.e.:

$$A_{\cos\phi_h}^{UU} = \frac{p_{\cos\phi_h}}{\langle\epsilon_1\rangle}, \qquad A_{\cos 2\phi_h}^{UU} = \frac{p_{\cos 2\phi_h}}{\langle\epsilon_2\rangle}, \qquad A_{\sin\phi_h}^{LU} = \frac{p_{\sin\phi_h}}{\langle\epsilon_3\rangle\lambda}. \tag{4}$$

The quantities $\langle\epsilon_i\rangle$ are the mean values of ϵ_i defined in Eq. (2) and calculated for each kinematic bin. The two central bins in ϕ_h have been excluded from the fit as will be explained in Section 6.2.

The same procedure is used to measure the azimuthal asymmetries for the hadrons binned simultaneously in x, z and p_T^h ("3d asymmetries").

5.2. Monte Carlo and acceptance corrections

In each kinematic bin and for each ϕ_h bin the azimuthal acceptance has been evaluated as:

$$a(\phi_{h_i}) = N_{rec}(\phi_{h_i})/N_{gen}(\phi_{h_i}), \tag{5}$$

where $N_{rec}(\phi_{h_i})$ is the number of reconstructed hadrons obtained from the Monte Carlo simulation and $N_{gen}(\phi_{h_i})$ is the corresponding number of generated hadrons. In order to obtain the number of reconstructed hadrons the same kinematic cuts, the same event reconstruction, and the same event and hadron selection as for the real data have been applied. Only the kinematic cuts are applied to evaluate the number of generated hadrons.

The simulation involves the full COMPASS Monte Carlo chain, namely: the generation of the DIS event, the propagation of the event inside the apparatus, and the reconstruction of particle tracks. The LEPTO generator [22] is used for the first step. The interactions between particles and materials and the detectors response are simulated using COMGEANT, a software based on GEANT3 [23] and developed inside the Collaboration to describe the COMPASS set-up and which also includes trigger efficiencies, while detector efficiencies are simulated at CORAL level. The package CORAL [24] is used to perform the track reconstruction and it is the same program used for the real data. It has been carefully checked that the Monte Carlo simulation gives a good description of the apparatus.

Starting from the distributions obtained using the default LEPTO setting, different tunings of the LEPTO parameters and also different sets of PDFs, already tested in other COMPASS analysis [25], have been used. The CTEQ5 [26] PDF set and the tuning of Ref. [25] have been adopted for the extraction of the acceptances.

The ratios between the distributions for real and for Monte Carlo events are shown in Fig. 4 as a function of the DIS variables, and in Fig. 5 as a function of the hadron variables. The agreement is satisfactory and gives confidence in the quality of the apparatus description used in the simulations. A typical hadron azimuthal distribution from raw data $N(\phi_h)$, the corresponding acceptance from the Monte Carlo simulation $a(\phi_h)$, and the corrected distribution $N_{corr}(\phi_h)$ are shown in Fig. 6 as a function of ϕ_h.

Eq. (3) shows that the relevant part of the acceptance is the one containing $\cos\phi_h$, $\cos 2\phi_h$ and $\sin\phi_h$ modulations. The amplitudes of these azimuthal modulations, which are essentially the corrections given by the Monte Carlo, have been evaluated and their trend has been studied as a function of the various kinematic variables. It has been found that the largest corrections, up to about 15%, have to be applied to the $\cos\phi_h$ modulations. The $\cos 2\phi_h$ corrections are of the order of a few percent and the $\sin\phi_h$ corrections are negligible.
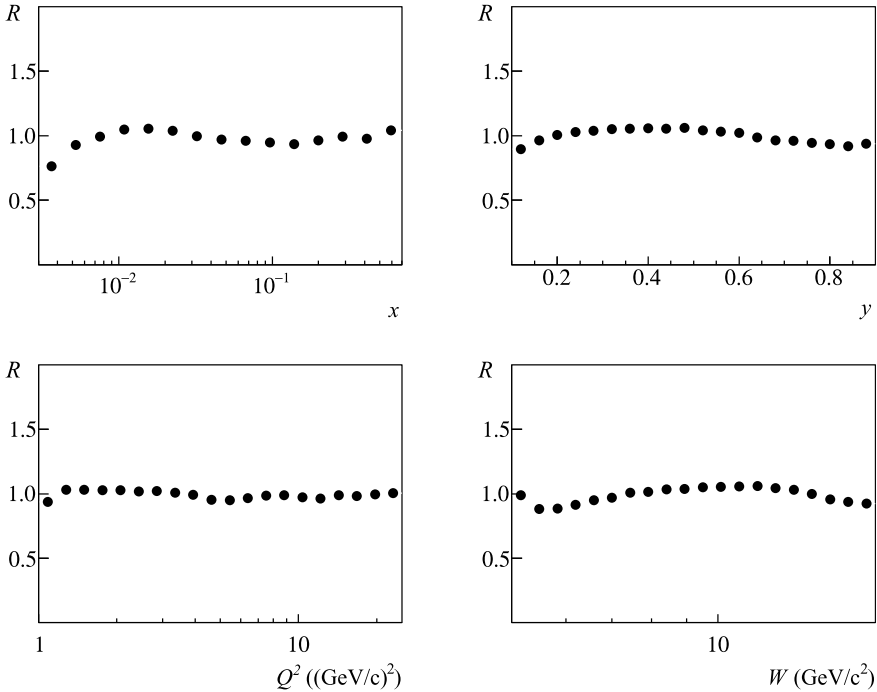
Fig. 4. Ratio R between data and Monte Carlo events distributions for x, y, Q^2 and W.

A priory the acceptance function $a(\phi_h, \vec{v})$ evaluated in a particular bin of a specific variable $(x, z, p_T^h, \ldots)$ could still depend on some geometrical observable t like the azimuthal or polar angle of the scattered muon or on some other kinematic variables. It has been verified that this is not the case. When extracting $a(\phi_h, \vec{v}, t)$ in bins of t, the resulting azimuthal asymmetries differ on average from those extracted through integration over t by less than one standard deviation of the statistical uncertainty, and also significantly less than the final systematic uncertainty.

6. Systematic studies

Several possible systematic effects have been investigated. The most relevant studies are described in this section. Some effects turned out to have a negligible impact on the results and thus were not included in the evaluation of the final systematic uncertainties.

6.1. Resolution effects

Due to the finite resolution of the detectors and of the tracking, the reconstructed values of some kinematic variables could result in a migration of an event (or hadron) from one bin to an adjacent bin. This effect can dilute the measured asymmetries with respect to the true ones. It has been evaluated using a Monte Carlo event sample with a $\cos\phi_h$ modulation with an amplitude linearly decreasing as a function of z from 0 to a value of -0.5. It has been found that the difference between the extracted amplitudes and the generated ones is always less than 1%, and thus it was neglected in the calculation of the systematic uncertainties.
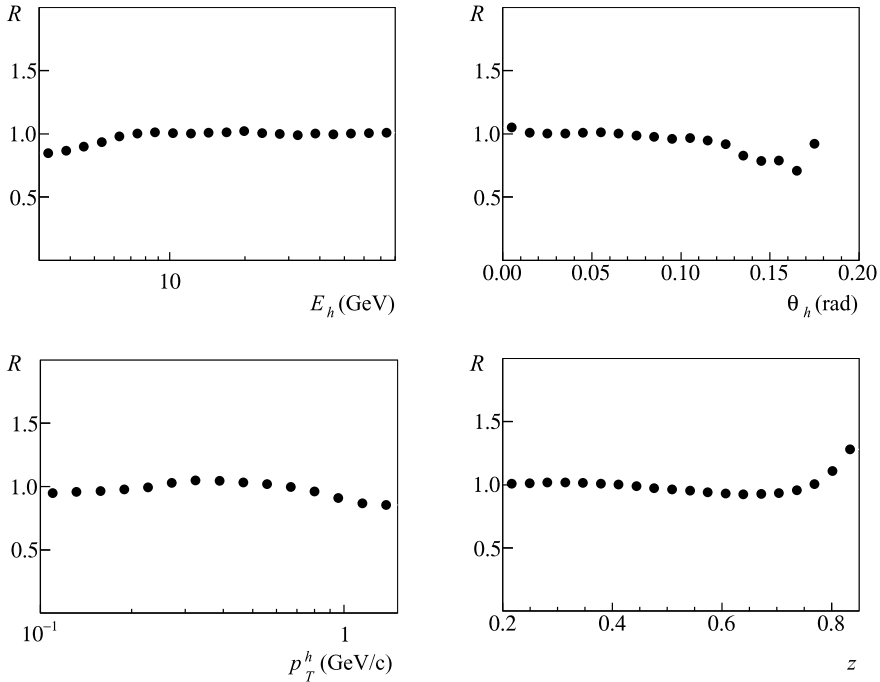
Fig. 5. Ratio R between data and Monte Carlo hadrons distributions for the energy, the polar angle calculated in the laboratory system, p_T^h and z.

6.2. Radiative effects

Radiative photons emitted from the lepton modify the reconstructed virtual photon 4-momentum with respect to the 4-momentum of the true virtual photon exchanged in the muon–nucleon interaction. This introduces a bias in the azimuthal distributions, since the reconstructed virtual photon direction in the lepton scattering plane is always at larger angles than that of the true virtual photon.

The effect of radiative corrections on the measured asymmetries is expected to be small for this analysis, because requirement of at least one hadron in the final state limits the radiative corrections to those for the inelastic part of the $\gamma^* N$ cross-section. In addition, the use of a muon beam results in further reduction of radiative corrections. Nevertheless, the effect has been evaluated by means of Monte Carlo simulations using a dedicated software (RADGEN [27]) in combination with LEPTO. The correction turns out to be negligible for the $\cos 2\phi_h$ modulation and is small (at most few percent in the high x region) for the $\cos \phi_h$ modulation, and almost of the same size for positive and for negative hadrons. The same conclusion has been drawn by performing an analytic calculation [28] which gives negligible effects ($\lesssim 1\%$ for the $\cos \phi_h$ modulation) in the COMPASS environment. For these reasons the radiative corrections have not been applied to the measured asymmetries and not included in the systematic uncertainties.

The azimuthal distributions of hadrons are affected by the contamination of electrons/positrons coming from the conversion of the radiated photons. The kinematics of the process is such that the contribution is present only in the two ϕ_h bins closest to $\phi_h = 0$ ($0 \le \phi_h < \pi/8$ and
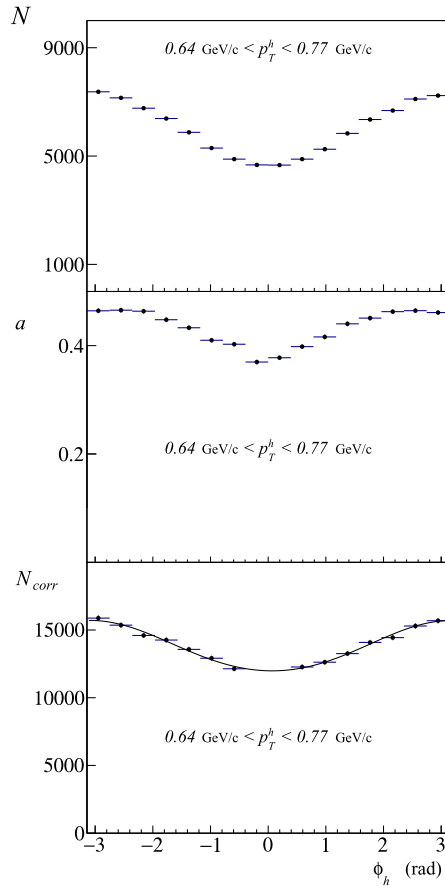
Fig. 6. Measured azimuthal distribution N, azimuthal acceptance a and measured azimuthal distribution corrected by the acceptance N_{corr} in one of the p_T^h bins for positive hadrons.

$15\pi/8 \le \phi_h < 2\pi$). In order to avoid corrections depending on the Monte Carlo description of the radiative effects, these two bins have been excluded in the extraction of the azimuthal asymmetries.

6.3. Acceptance corrections

The asymmetries have also been extracted using two other Monte Carlo event samples. They use the same description of the apparatus but different tuning of the LEPTO generator. They both compare satisfactorily with the data and can be considered as "extreme cases" as shown in Fig. 7. Since the acceptance is approximately flat in the selected kinematic region the results are similar as shown for example in Fig. 8. The difference between the amplitudes of the azimuthal modulations extracted from the data corrected with the acceptance calculated using the three different Monte Carlo samples turned out to be slightly larger than the statistical errors of the results. These differences have been included in the systematic uncertainties.
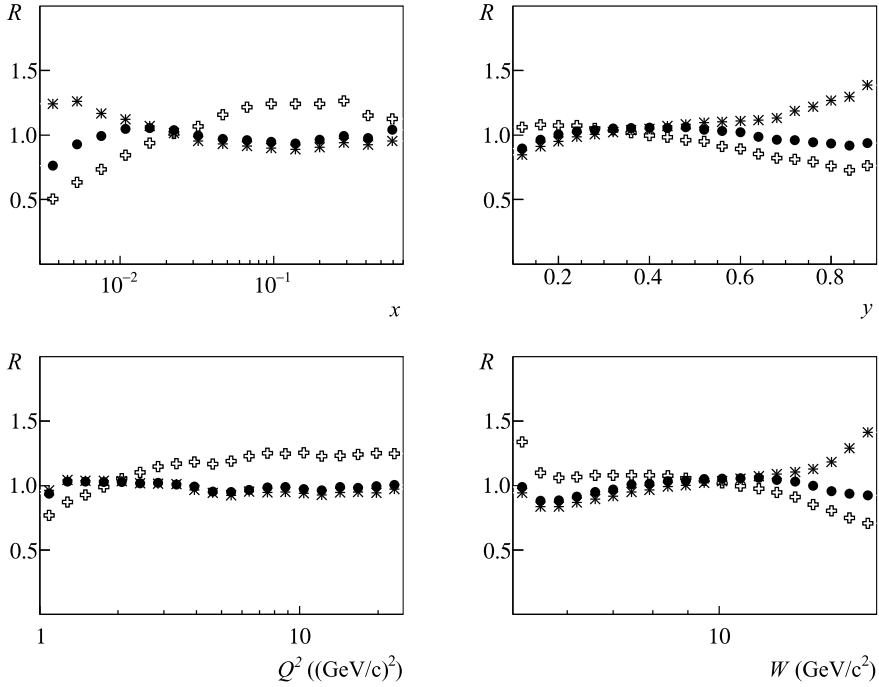
Fig. 7. Ratio R between data and Monte Carlo events distributions. The different markers correspond to the three different Monte Carlo tunings which have been used to evaluate the acceptance. The full points are the same as in Fig. 4.
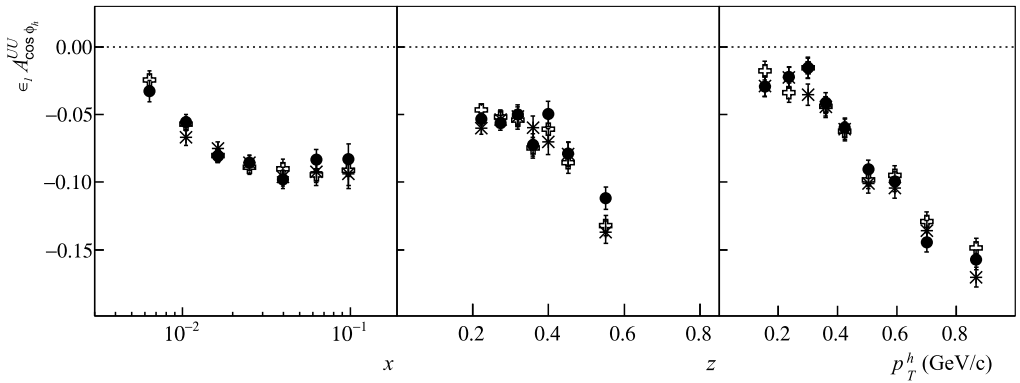
Fig. 8. The amplitudes of the $\cos\phi_h$ modulations ($\epsilon_1 A_{\cos\phi_h}^{UU}$) for positive hadrons extracted using the acceptance corrections from the three Monte Carlo samples of Fig. 7.

6.4. Stability of the results

The same azimuthal asymmetries have also been extracted from a different data sample, namely four different weeks of the 2004 run when the target was longitudinally polarised. A dedicated Monte Carlo simulation has been performed to describe the apparatus, which was somewhat different from the one used for the present analysis. The magnetic field in the

target region was different and the beam line was shifted to account for it. Also the triggers were changed and some detectors parameters were differently tuned. The asymmetries extracted from these data have been compared with the final ones and the difference between them (on average, one statistical standard deviation) has been included in the systematic uncertainties.

6.5. Detector efficiency

A contribution to the azimuthal modulations of the acceptances could be due to detector inefficiencies in regions where there are less redundancies in the track reconstruction. A Monte Carlo study has been performed in order to study the azimuthal modulations of acceptance assuming certain detectors to be inefficient. The ratio between the azimuthal distributions of the hadrons reconstructed with reduced efficiency and with nominal detector conditions has been obtained for every kinematic bin. As a result, it has been found that only the $\cos\phi_h$ azimuthal modulation changes, in particular in the high x region, where the effect is up to 0.5 of the statistical uncertainty. This contribution is included in the systematic uncertainties.

6.6. Evaluation of the systematic uncertainties

The three important contributions to the systematic uncertainties (acceptance corrections, period compatibility and, to a lesser extent, detector inefficiencies) have been added up in quadrature and the final systematic uncertainty σ_{syst} has been evaluated for the 1d asymmetries to be twice as large as the statistical ones σ_{stat} independently from the kinematic region. The same systematic studies have been performed also for the 3d asymmetries evaluated in bins of x, z and p_T^h. For these asymmetries the total systematic uncertainty has been evaluated to be $\sigma_{syst} \simeq \sigma_{stat}$.

7. Results

7.1. Asymmetries for separate binning in x, z or p_T^h

The results obtained binning the data in the kinematic variables x, z or p_T^h (integrated asymmetries) are listed in Tables 2–4 and shown in Fig. 9 for $A_{\sin\phi_h}^{LU}$, in Fig. 10 for $A_{\cos\phi_h}^{UU}$ and in Fig. 11 for $A_{\cos 2\phi_h}^{UU}$. The red points and the black triangles show the asymmetries for positive and negative hadrons, respectively. The error bars represent statistical uncertainties. As described in the previous section, the systematic point-to-point uncertainties are estimated to be as large as twice the statistical ones when including the uncertainty due to the Monte Carlo generators used to estimate the acceptance.

As can be seen in Fig. 9, the $A_{\sin\phi_h}^{LU}$ asymmetries are small, slightly positive, increasing with z, and almost constant in x and p_T^h within statistical errors. Similar results were obtained for π^+ by the CLAS Collaboration [29] using an electron beam of 4.3 GeV/c and a proton target, and for charged pions by the HERMES Collaboration [30] with a 27.6 GeV/c positron beam and a proton target. Given the different targets and the different kinematic regions a quantitative comparison with the present results is not straightforward.

The $A_{\cos\phi_h}^{UU}$ asymmetry given in Fig. 10 is large and negative for both positive and negative hadrons, with larger absolute values for positive hadrons. The dependence on the kinematic variables is strong, in particular on z and p_T^h. The asymmetries as a function of z are almost constant

Table 2

$A^{LU}_{\sin\phi_h}$ asymmetries for positive and negative hadrons as functions of x, z and p^h_T. For this and the following tables the mean kinematic values refer to the h^+ sample.

x range	$\langle x\rangle$	$\langle Q^2\rangle$ $(\mathrm{GeV}/c)^2$	$\langle z\rangle$	$\langle p^h_T\rangle$ (GeV/c)	$A^{LU}_{\sin\phi_h}$ (h^+)	$A^{LU}_{\sin\phi_h}$ (h^-)
0.003–0.008	0.006	1.26	0.35	0.47	$0.024\pm0.008\pm0.016$	$0.021\pm0.008\pm0.016$
0.008–0.013	0.011	1.52	0.35	0.47	$0.022\pm0.007\pm0.014$	$0.012\pm0.007\pm0.014$
0.013–0.020	0.016	1.81	0.35	0.46	$-0.009\pm0.008\pm0.016$	$-0.003\pm0.009\pm0.018$
0.020–0.032	0.025	2.60	0.35	0.46	$0.021\pm0.009\pm0.018$	$0.024\pm0.010\pm0.020$
0.032–0.050	0.040	4.18	0.35	0.46	$-0.003\pm0.012\pm0.024$	$0.024\pm0.013\pm0.026$
0.050–0.080	0.063	6.52	0.35	0.46	$0.000\pm0.014\pm0.028$	$0.013\pm0.015\pm0.030$
0.080–0.130	0.098	11.24	0.35	0.47	$-0.000\pm0.018\pm0.036$	$-0.043\pm0.021\pm0.042$

z range	$\langle x\rangle$	$\langle Q^2\rangle$ $(\mathrm{GeV}/c)^2$	$\langle z\rangle$	$\langle p^h_T\rangle$ (GeV/c)	$A^{LU}_{\sin\phi_h}$ (h^+)	$A^{LU}_{\sin\phi_h}$ (h^-)
0.20–0.25	0.027	3.06	0.22	0.43	$-0.001\pm0.007\pm0.014$	$-0.005\pm0.007\pm0.014$
0.25–0.30	0.027	3.07	0.27	0.45	$0.000\pm0.007\pm0.014$	$0.006\pm0.009\pm0.018$
0.30–0.34	0.027	3.05	0.32	0.46	$0.022\pm0.011\pm0.022$	$0.021\pm0.011\pm0.022$
0.34–0.38	0.027	3.06	0.36	0.47	$0.013\pm0.012\pm0.024$	$0.003\pm0.013\pm0.026$
0.38–0.42	0.027	3.05	0.40	0.48	$0.019\pm0.014\pm0.028$	$0.020\pm0.015\pm0.030$
0.42–0.49	0.027	3.01	0.45	0.49	$0.020\pm0.013\pm0.026$	$0.017\pm0.014\pm0.028$
0.49–0.63	0.027	2.95	0.55	0.51	$0.000\pm0.012\pm0.024$	$0.030\pm0.013\pm0.026$
0.63–0.85	0.026	2.78	0.72	0.50	$0.052\pm0.015\pm0.030$	$0.066\pm0.016\pm0.032$

p^h_T range (GeV/c)	$\langle x\rangle$	$\langle Q^2\rangle$ $(\mathrm{GeV}/c)^2$	$\langle z\rangle$	$\langle p^h_T\rangle$ (GeV/c)	$A^{LU}_{\sin\phi_h}$ (h^+)	$A^{LU}_{\sin\phi_h}$ (h^-)
0.10–0.20	0.027	3.01	0.33	0.16	$0.001\pm0.011\pm0.022$	$0.012\pm0.012\pm0.024$
0.20–0.27	0.027	2.98	0.34	0.24	$0.015\pm0.011\pm0.022$	$0.017\pm0.012\pm0.024$
0.27–0.33	0.027	2.96	0.34	0.30	$-0.003\pm0.011\pm0.022$	$0.027\pm0.012\pm0.024$
0.33–0.39	0.027	2.97	0.34	0.36	$0.017\pm0.011\pm0.022$	$0.020\pm0.012\pm0.024$
0.39–0.46	0.027	3.00	0.34	0.43	$0.003\pm0.011\pm0.022$	$0.013\pm0.011\pm0.022$
0.46–0.55	0.027	3.02	0.35	0.50	$0.014\pm0.010\pm0.020$	$0.023\pm0.011\pm0.022$
0.55–0.64	0.027	3.07	0.36	0.59	$0.013\pm0.011\pm0.022$	$0.019\pm0.012\pm0.024$
0.64–0.77	0.027	3.10	0.37	0.70	$0.021\pm0.011\pm0.022$	$0.007\pm0.011\pm0.022$
0.77–1.00	0.027	3.16	0.39	0.87	$0.006\pm0.011\pm0.022$	$-0.034\pm0.011\pm0.022$

up to $z \simeq 0.5$ and increase in absolute value at larger z up to 0.15. They show a similar behaviour as a function of p^h_T: the asymmetries are almost constant up to $p^h_T \simeq 0.4$ GeV/c and then increase rapidly in absolute value. The comparison with most of the existing data is difficult because of the different kinematic ranges. Moreover, the asymmetries have been measured as functions of different variables and without charge separation. This is not the case for the recently published results by the HERMES experiment [15], which give the asymmetries as a function of x, y, z and p^h_T both for proton and deuteron targets and for charged and identified hadrons. However, a quantitative comparison is still difficult because HERMES measurements correspond to smaller Q^2 values and to larger x, although the x-dependence of $A^{UU}_{\cos\phi_h}$ asymmetry from HERMES is in qualitative agreement with the present measurement. In particular, the HERMES results also show larger (and negative) asymmetries for positive hadrons in the overlapping x region. Because of the different x range, the HERMES mean values are smaller but the data show z and p^h_T dependencies similar to that shown in Fig. 10. When compared to theoretical calculations and

Table 3

$A_{\cos\phi_h}^{UU}$ asymmetries for positive and negative hadrons as functions of x, z and p_T^h.

x range	$\langle x\rangle$	$\langle Q^2\rangle$ (GeV/c)^2	$\langle z\rangle$	$\langle p_T^h\rangle$ (GeV/c)	$A_{\cos\phi_h}^{UU}$ (h^+)	$A_{\cos\phi_h}^{UU}$ (h^-)
0.003–0.008	0.006	1.26	0.35	0.47	$-0.018\pm0.005\pm0.010$	$-0.020\pm0.005\pm0.010$
0.008–0.013	0.011	1.52	0.35	0.47	$-0.037\pm0.003\pm0.006$	$-0.018\pm0.003\pm0.006$
0.013–0.020	0.016	1.81	0.35	0.46	$-0.043\pm0.002\pm0.004$	$-0.032\pm0.003\pm0.006$
0.020–0.032	0.025	2.60	0.35	0.46	$-0.050\pm0.003\pm0.006$	$-0.035\pm0.003\pm0.006$
0.032–0.050	0.040	4.18	0.35	0.46	$-0.059\pm0.003\pm0.006$	$-0.043\pm0.004\pm0.008$
0.050–0.080	0.063	6.52	0.35	0.46	$-0.056\pm0.004\pm0.008$	$-0.039\pm0.004\pm0.008$
0.080–0.130	0.098	11.24	0.35	0.47	$-0.061\pm0.005\pm0.010$	$-0.045\pm0.006\pm0.012$

z range	$\langle x\rangle$	$\langle Q^2\rangle$ (GeV/c)^2	$\langle z\rangle$	$\langle p_T^h\rangle$ (GeV/c)	$A_{\cos\phi_h}^{UU}$ (h^+)	$A_{\cos\phi_h}^{UU}$ (h^-)
0.20–0.25	0.027	3.06	0.22	0.43	$-0.034\pm0.002\pm0.004$	$-0.021\pm0.002\pm0.004$
0.25–0.30	0.027	3.07	0.27	0.45	$-0.030\pm0.003\pm0.006$	$-0.026\pm0.003\pm0.006$
0.30–0.34	0.027	3.05	0.32	0.46	$-0.034\pm0.004\pm0.008$	$-0.014\pm0.004\pm0.008$
0.34–0.38	0.027	3.06	0.36	0.47	$-0.034\pm0.004\pm0.008$	$-0.026\pm0.004\pm0.008$
0.38–0.42	0.027	3.05	0.40	0.48	$-0.033\pm0.005\pm0.010$	$-0.014\pm0.005\pm0.010$
0.42–0.49	0.027	3.01	0.45	0.49	$-0.051\pm0.004\pm0.008$	$-0.026\pm0.005\pm0.010$
0.49–0.63	0.027	2.95	0.55	0.51	$-0.081\pm0.004\pm0.008$	$-0.056\pm0.004\pm0.008$
0.63–0.85	0.026	2.78	0.72	0.50	$-0.150\pm0.005\pm0.010$	$-0.130\pm0.005\pm0.010$

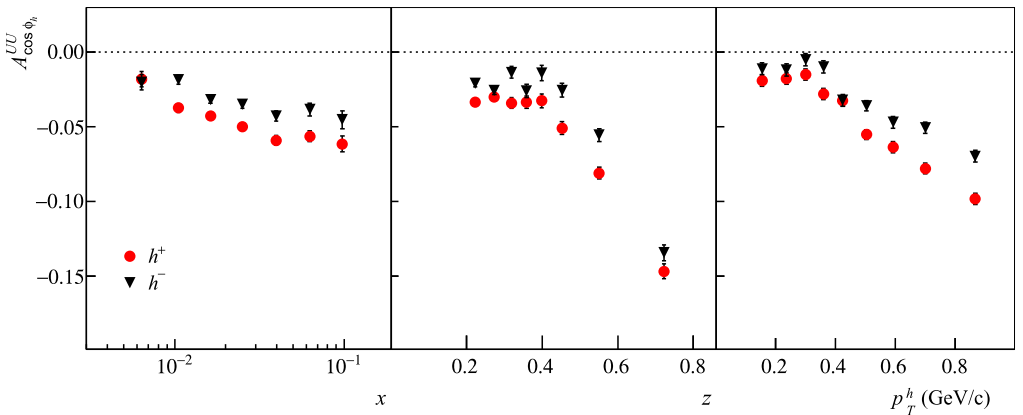| p_T^h range (GeV/c)	$\langle x\rangle$	$\langle Q^2\rangle$ (GeV/c)^2	$\langle z\rangle$	$\langle p_T^h\rangle$ (GeV/c)	$A_{\cos\phi_h}^{UU}$ (h^+)	$A_{\cos\phi_h}^{UU}$ (h^-)
0.10–0.20	0.027	3.01	0.33	0.16	$-0.019\pm0.004\pm0.008$	$-0.011\pm0.004\pm0.008$
0.20–0.27	0.027	2.98	0.34	0.24	$-0.018\pm0.004\pm0.008$	$-0.012\pm0.004\pm0.008$
0.27–0.33	0.027	2.96	0.34	0.30	$-0.015\pm0.004\pm0.008$	$-0.005\pm0.004\pm0.008$
0.33–0.39	0.027	2.97	0.34	0.36	$-0.028\pm0.004\pm0.008$	$-0.010\pm0.004\pm0.008$
0.39–0.46	0.027	3.00	0.34	0.43	$-0.033\pm0.004\pm0.008$	$-0.032\pm0.004\pm0.008$
0.46–0.55	0.027	3.02	0.35	0.50	$-0.055\pm0.003\pm0.006$	$-0.036\pm0.004\pm0.008$
0.55–0.64	0.027	3.07	0.36	0.59	$-0.064\pm0.004\pm0.008$	$-0.047\pm0.004\pm0.008$
0.64–0.77	0.027	3.10	0.37	0.70	$-0.078\pm0.004\pm0.008$	$-0.051\pm0.004\pm0.008$
0.77–1.00	0.027	3.16	0.39	0.87	$-0.098\pm0.004\pm0.008$	$-0.070\pm0.004\pm0.008$
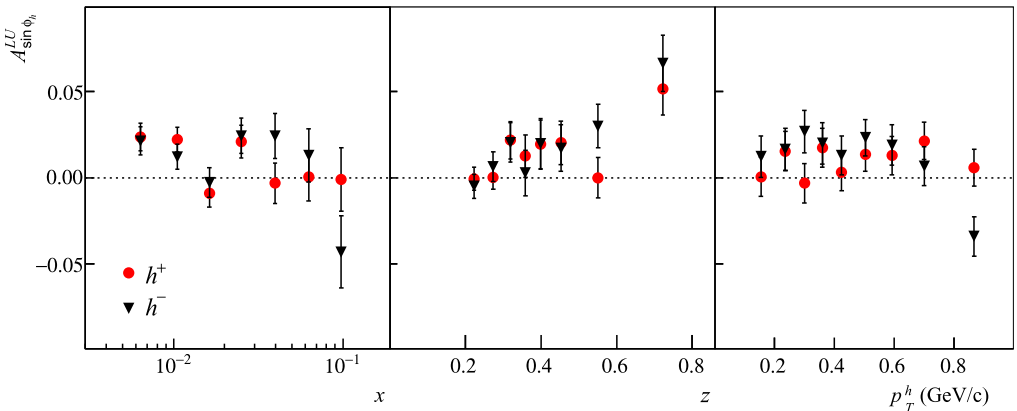
Fig. 9. $A_{\sin\phi_h}^{LU}$ integrated asymmetries for positive (red points) and negative (black triangles) hadrons as functions of x, z and p_T^h. The error bars show statistical uncertainties only.

Table 4
$A^{UU}_{\cos 2\phi_h}$ asymmetries for positive and negative hadrons as functions of x, z and p^h_T.

x range	$\langle x \rangle$	$\langle Q^2 \rangle$ (GeV/c)^2	$\langle z \rangle$	$\langle p^h_T \rangle$ (GeV/c)	$A^{UU}_{\cos 2\phi_h}$ (h^+)	$A^{UU}_{\cos 2\phi_h}$ (h^-)
0.003–0.008	0.006	1.26	0.35	0.47	$0.067 \pm 0.010 \pm 0.020$	$0.064 \pm 0.010 \pm 0.020$
0.008–0.013	0.011	1.52	0.35	0.47	$0.037 \pm 0.006 \pm 0.012$	$0.066 \pm 0.006 \pm 0.012$
0.013–0.020	0.016	1.81	0.35	0.46	$0.029 \pm 0.005 \pm 0.010$	$0.044 \pm 0.005 \pm 0.010$
0.020–0.032	0.025	2.60	0.35	0.46	$0.023 \pm 0.005 \pm 0.010$	$0.048 \pm 0.005 \pm 0.010$
0.032–0.050	0.040	4.18	0.35	0.46	$0.015 \pm 0.007 \pm 0.014$	$0.025 \pm 0.007 \pm 0.014$
0.050–0.080	0.063	6.52	0.35	0.46	$0.009 \pm 0.008 \pm 0.016$	$0.022 \pm 0.008 \pm 0.016$
0.080–0.130	0.098	11.24	0.35	0.47	$-0.004 \pm 0.010 \pm 0.020$	$0.005 \pm 0.010 \pm 0.020$

z range	$\langle x \rangle$	$\langle Q^2 \rangle$ (GeV/c)^2	$\langle z \rangle$	$\langle p^h_T \rangle$ (GeV/c)	$A^{UU}_{\cos 2\phi_h}$ (h^+)	$A^{UU}_{\cos 2\phi_h}$ (h^-)
0.20–0.25	0.027	3.06	0.22	0.43	$0.010 \pm 0.005 \pm 0.010$	$0.014 \pm 0.005 \pm 0.010$
0.25–0.30	0.027	3.07	0.27	0.45	$0.013 \pm 0.005 \pm 0.010$	$0.020 \pm 0.006 \pm 0.012$
0.30–0.34	0.027	3.05	0.32	0.46	$0.026 \pm 0.007 \pm 0.014$	$0.048 \pm 0.008 \pm 0.016$
0.34–0.38	0.027	3.06	0.36	0.47	$0.037 \pm 0.008 \pm 0.016$	$0.058 \pm 0.009 \pm 0.018$
0.38–0.42	0.027	3.05	0.40	0.48	$0.036 \pm 0.009 \pm 0.018$	$0.077 \pm 0.010 \pm 0.020$
0.42–0.49	0.027	3.01	0.45	0.49	$0.034 \pm 0.008 \pm 0.016$	$0.066 \pm 0.009 \pm 0.018$
0.49–0.63	0.027	2.95	0.55	0.51	$0.070 \pm 0.008 \pm 0.016$	$0.110 \pm 0.009 \pm 0.018$
0.63–0.85	0.026	2.78	0.72	0.50	$0.035 \pm 0.010 \pm 0.020$	$0.088 \pm 0.010 \pm 0.020$

p^h_T range (GeV/c)	$\langle x \rangle$	$\langle Q^2 \rangle$ (GeV/c)^2	$\langle z \rangle$	$\langle p^h_T \rangle$ (GeV/c)	$A^{UU}_{\cos 2\phi_h}$ (h^+)	$A^{UU}_{\cos 2\phi_h}$ (h^-)
0.10–0.20	0.027	3.01	0.33	0.16	$0.009 \pm 0.008 \pm 0.016$	$0.020 \pm 0.008 \pm 0.016$
0.20–0.27	0.027	2.98	0.34	0.24	$0.028 \pm 0.008 \pm 0.016$	$0.030 \pm 0.008 \pm 0.016$
0.27–0.33	0.027	2.96	0.34	0.30	$0.055 \pm 0.008 \pm 0.016$	$0.048 \pm 0.008 \pm 0.016$
0.33–0.39	0.027	2.97	0.34	0.36	$0.041 \pm 0.007 \pm 0.014$	$0.056 \pm 0.008 \pm 0.016$
0.39–0.46	0.027	3.00	0.34	0.43	$0.043 \pm 0.007 \pm 0.014$	$0.053 \pm 0.008 \pm 0.016$
0.46–0.55	0.027	3.02	0.35	0.50	$0.029 \pm 0.007 \pm 0.014$	$0.053 \pm 0.007 \pm 0.014$
0.55–0.64	0.027	3.07	0.36	0.59	$0.015 \pm 0.008 \pm 0.016$	$0.038 \pm 0.008 \pm 0.016$
0.64–0.77	0.027	3.10	0.37	0.70	$0.006 \pm 0.007 \pm 0.014$	$0.051 \pm 0.008 \pm 0.016$
0.77–1.00	0.027	3.16	0.39	0.87	$0.012 \pm 0.008 \pm 0.016$	$0.046 \pm 0.008 \pm 0.016$

Fig. 10. $A^{UU}_{\cos\phi_h}$ integrated asymmetries for positive (red points) and for negative (black triangles) hadrons as functions of x, z and p^h_T. The error bars show statistical uncertainties only.

Fig. 11. $A^{UU}_{\cos 2\phi_h}$ integrated asymmetries for positive (red points) and negative (black triangles) hadrons as functions of x, z and p^h_T. The error bars show statistical uncertainties only.
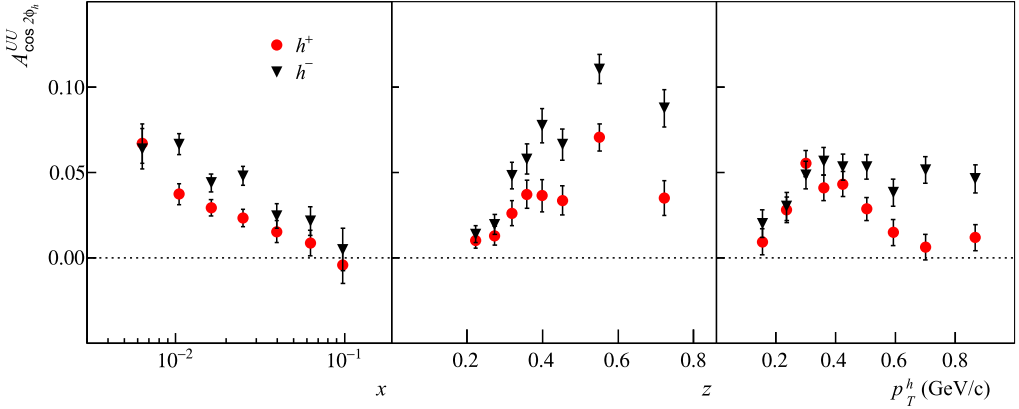
predictions [31], the agreement is not satisfactory, in particular for the z and p^h_T dependencies and work to understand the discrepancies is ongoing.

The $A^{UU}_{\cos 2\phi_h}$ asymmetries are also significantly different from zero and different for positive and negative hadrons. They both are positive and larger for negative hadrons, over all the measured range. Again there is a strong dependence on the kinematic variables. In this case the asymmetry decreases with x and it increases as functions of z and p^h_T, but only up to $z \simeq 0.6$ and $p^h_T \simeq 0.4$ GeV/c. Strong dependencies on the kinematic variables are also present in the HER-MES results [15]. First attempts to describe the observed behaviour in terms of the Cahn effect that is expected to dominate at small x and the Boer–Mulders effect [32] could not reproduce the data well, and in particular the p^h_T dependence (the preliminary results were even not included in the fit) which was expected to be almost linear.

7.2. Asymmetries for simultaneous binning in x, z and p^h_T

In order to investigate the observed dependencies on kinematic variables the azimuthal asymmetries have also been extracted binning simultaneously the data in bins of x, z and p^h_T (3d asymmetries). This would also reduce the possible residual impact of the overall detector acceptance on the 1d results which is included in the systematic uncertainty. The results for the four x bins are given in Tables 5–12. The results for $A^{UU}_{\cos \phi_h}$ for positive (red points) and negative (black triangles) hadrons are shown in Fig. 12. The results for $A^{UU}_{\cos 2\phi_h}$ are shown in Fig. 13 and again the error bars represent only the statistical uncertainties. The 3d asymmetries have also been evaluated for $A^{LU}_{\sin \phi_h}$ but no particular effect could be noticed due to the larger statistical uncertainties. It has also been checked that the projection of the asymmetries on any of the three kinematic variables is consistent with the results for the integrated asymmetries given in the previous section.

From the results shown in Fig. 12 interesting information on $A^{UU}_{\cos \phi_h}$ can be obtained. Looking at the x dependence in the z and p^h_T bins, it is clear that the large negative values at small x are obtained for hadrons with $0.55 < z < 0.85$, while for smaller z the asymmetries are either very small (0.1 GeV/$c < p^h_T < 0.5$ GeV/c) or indicate a different x dependence ($p^h_T > 0.5$ GeV/c). Also, as can be seen in the figure, the absolute values of the asymmetries for $z < 0.55$ increase

Fig. 12. $A^{UU}_{\cos\phi_h}$ asymmetries for positive (red points) and negative (black triangles) hadrons as a function of x for the different bins in p^h_T (from left to right) and z (from bottom to top). The error bars show statistical uncertainties only.
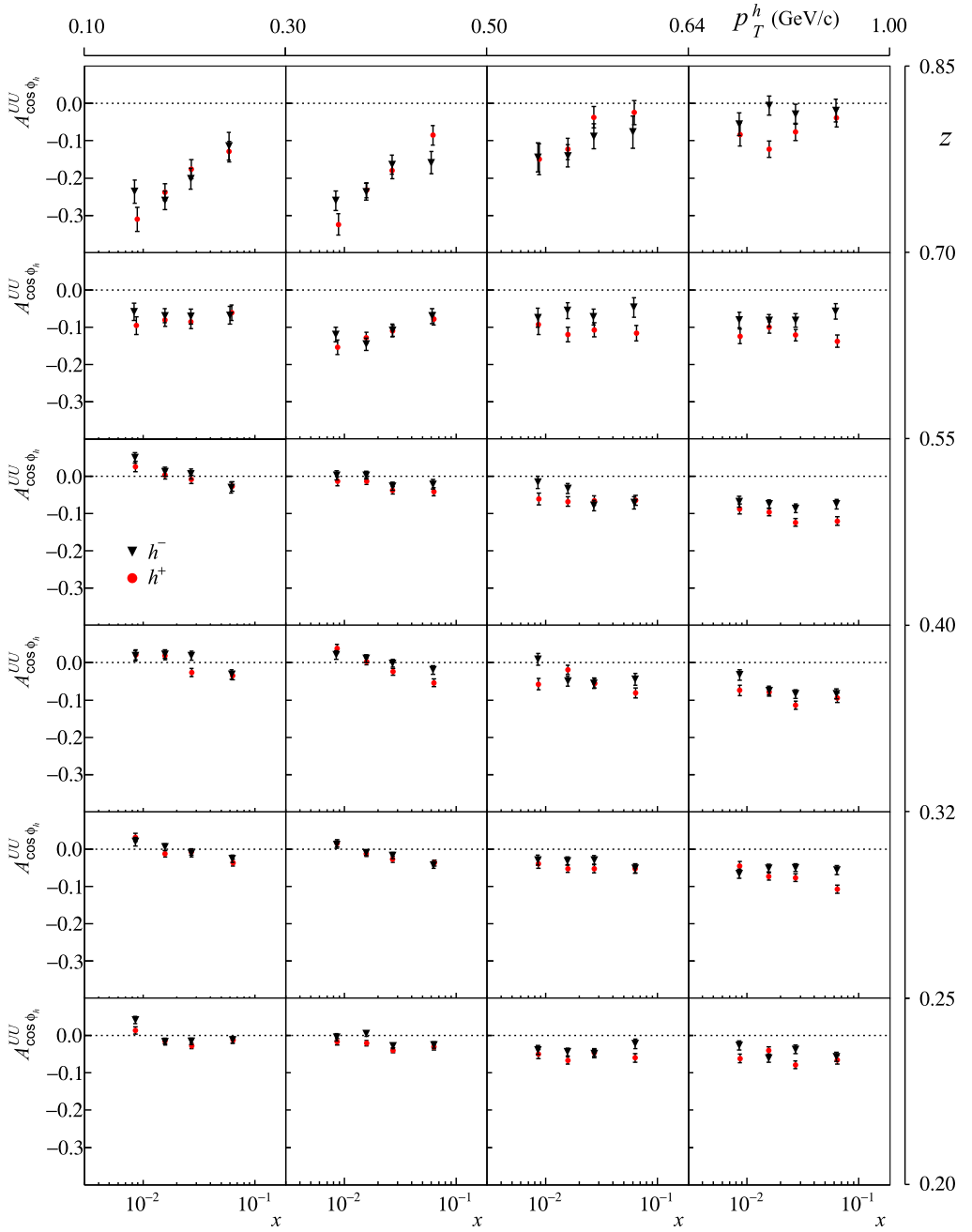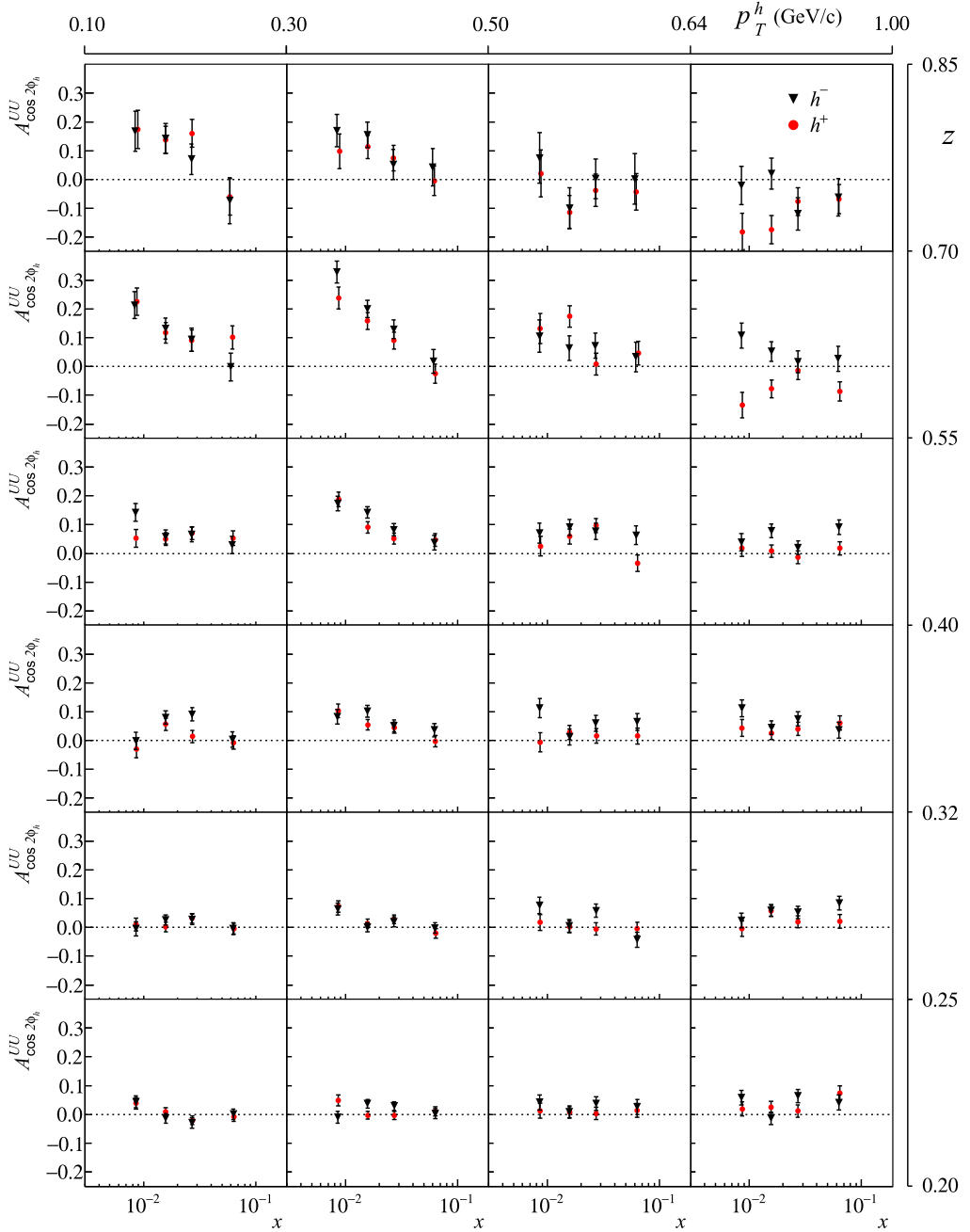
Fig. 13. $A^{UU}_{\cos 2\phi_h}$ asymmetries for positive (red points) and negative (black triangles) hadrons as a function of x for the different bins in p^h_T (from left to right) and z (from bottom to top). The error bars show statistical uncertainties only.
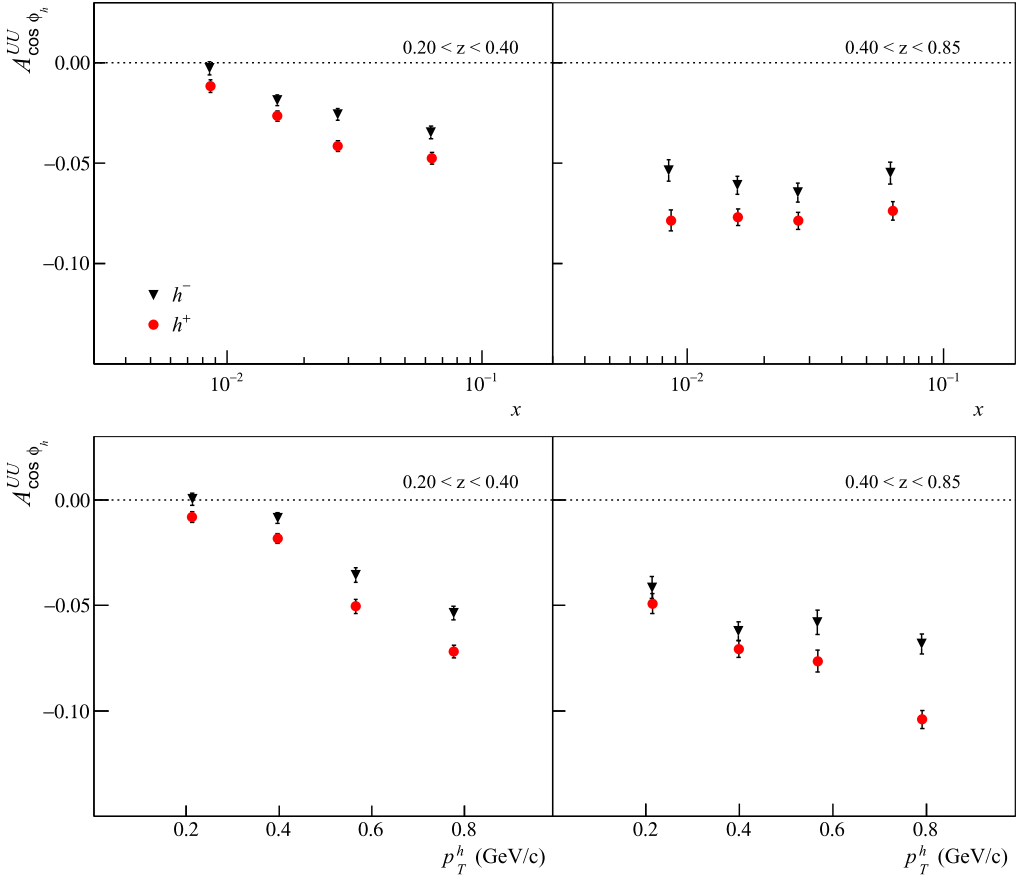
Fig. 14. $A_{\cos\phi_h}^{UU}$ as functions of x (top) and p_T^h (bottom) calculated for $0.2 < z < 0.4$ (left) and for $0.4 < z < 0.85$ (right). The error bars show statistical uncertainties only.

with p_T^h, and the large and negative values at large z in the 1d projection are mainly due to the values at small x and p_T^h. Summarising, the data suggest that there are different regimes and different dominant processes in the various regions of the (x, z, p_T^h) space and that a deeper phenomenological investigation is required.

Also $A_{\cos 2\phi_h}^{UU}$ shows a similarly strong dependence on the x, z and p_T^h variables, as can be seen in Fig. 13. The large positive asymmetry values in the low-x region in the 1d projection are mainly observed at small p_T^h values and large z values. For $p_T^h > 0.5$ GeV/c $A_{\cos 2\phi_h}^{UU}$ becomes smaller and shows a different x dependence.

The presence of two different regimes according to the z values appears very clearly in Fig. 14 and Fig. 15. Here the asymmetries have been calculated at low z ($0.2 < z < 0.4$) and at high z ($0.4 < z < 0.85$) and both the x and p_T^h dependencies of the $A_{\cos\phi_h}^{UU}$ and $A_{\cos 2\phi_h}^{UU}$ asymmetries are found to be significantly different. As a side remark we can remind that the low z behaviour is qualitatively reproduced by the existing fit and calculations [31,32], while the dependence at high z seems to be more difficult to be reproduced theoretically.

Fig. 15. $A^{UU}_{\cos 2\phi_h}$ as functions of x (top) and p^h_T (bottom) calculated for $0.2 < z < 0.4$ (left) and for $0.4 < z < 0.85$ (right). The error bars show statistical uncertainties only.

8. Conclusions

COMPASS has measured the azimuthal asymmetries in semi-inclusive DIS of polarised 160 GeV/c muons off an unpolarised isoscalar target, covering a broad x region down to $x = 0.003$. Results have been produced binning the data in x, z or p^h_T, integrating over the other two variables, and in a three-dimensional grid of the three variables x, z and p^h_T. The amplitude of the $\sin\phi_h$ modulation is positive and small with respect to the statistical uncertainties. The amplitude of the $\cos\phi_h$ and $\cos 2\phi_h$ modulations clearly show non-zero values and their dependencies over kinematical variables turns out to be very strong and not easy to be described in the present phenomenological framework. The new data can be used in multidimensional global analyses and constitute an important information for the understanding of the transverse momentum structure of the nucleon.

Table 5

$A^{UU}_{\cos\phi_h}$ 3d asymmetries for positive and negative hadrons in the first x bin ($0.003 < x < 0.012$). For this and the following tables the mean kinematic values refer to the h^+ sample.

z range	p_T^h range (GeV/c)	$\langle x \rangle$	$\langle Q^2 \rangle$ (GeV/c)	$\langle z \rangle$	$\langle p_T^h \rangle$ (GeV/c)	$A^{UU}_{\cos\phi_h}$ (h^+)	$A^{UU}_{\cos\phi_h}$ (h^-)
0.20–0.25	0.10–0.30	0.009	1.41	0.22	0.21	$0.014\pm0.010\pm0.010$	$0.041\pm0.010\pm0.010$
	0.30–0.50	0.009	1.41	0.22	0.40	$-0.017\pm0.009\pm0.009$	$-0.005\pm0.010\pm0.010$
	0.50–0.64	0.009	1.40	0.22	0.56	$-0.050\pm0.012\pm0.012$	$-0.039\pm0.012\pm0.012$
	0.64–1.00	0.009	1.42	0.22	0.78	$-0.062\pm0.011\pm0.011$	$-0.026\pm0.012\pm0.012$
0.25–0.32	0.10–0.30	0.009	1.41	0.28	0.21	$0.031\pm0.011\pm0.011$	$0.020\pm0.011\pm0.011$
	0.30–0.50	0.009	1.41	0.28	0.40	$0.016\pm0.009\pm0.009$	$0.012\pm0.010\pm0.010$
	0.50–0.64	0.009	1.41	0.28	0.57	$-0.039\pm0.013\pm0.013$	$-0.030\pm0.013\pm0.013$
	0.64–1.00	0.009	1.41	0.28	0.78	$-0.045\pm0.012\pm0.012$	$-0.066\pm0.012\pm0.012$
0.32–0.40	0.10–0.30	0.009	1.40	0.36	0.21	$0.021\pm0.013\pm0.013$	$0.019\pm0.014\pm0.014$
	0.30–0.50	0.009	1.40	0.36	0.40	$0.038\pm0.012\pm0.012$	$0.021\pm0.012\pm0.012$
	0.50–0.64	0.009	1.40	0.36	0.57	$-0.058\pm0.015\pm0.015$	$0.009\pm0.016\pm0.016$
	0.64–1.00	0.009	1.41	0.36	0.78	$-0.074\pm0.014\pm0.014$	$-0.033\pm0.014\pm0.014$
0.40–0.55	0.10–0.30	0.009	1.39	0.46	0.21	$0.026\pm0.014\pm0.014$	$0.050\pm0.014\pm0.014$
	0.30–0.50	0.009	1.40	0.46	0.40	$-0.013\pm0.012\pm0.012$	$0.003\pm0.012\pm0.012$
	0.50–0.64	0.009	1.41	0.46	0.57	$-0.061\pm0.016\pm0.016$	$-0.016\pm0.017\pm0.017$
	0.64–1.00	0.009	1.41	0.47	0.79	$-0.087\pm0.014\pm0.014$	$-0.068\pm0.015\pm0.015$
0.55–0.70	0.10–0.30	0.009	1.36	0.61	0.22	$-0.096\pm0.024\pm0.024$	$-0.059\pm0.023\pm0.023$
	0.30–0.50	0.009	1.38	0.62	0.40	$-0.154\pm0.019\pm0.019$	$-0.120\pm0.019\pm0.019$
	0.50–0.64	0.009	1.39	0.61	0.57	$-0.093\pm0.026\pm0.026$	$-0.074\pm0.026\pm0.026$
	0.64–1.00	0.009	1.41	0.62	0.80	$-0.124\pm0.020\pm0.020$	$-0.080\pm0.020\pm0.020$
0.70–0.85	0.10–0.30	0.009	1.35	0.77	0.22	$-0.310\pm0.032\pm0.032$	$-0.236\pm0.031\pm0.031$
	0.30–0.50	0.009	1.37	0.77	0.39	$-0.325\pm0.029\pm0.029$	$-0.260\pm0.026\pm0.026$
	0.50–0.64	0.009	1.38	0.77	0.57	$-0.149\pm0.041\pm0.041$	$-0.145\pm0.039\pm0.039$
	0.64–1.00	0.009	1.39	0.77	0.80	$-0.083\pm0.031\pm0.031$	$-0.056\pm0.031\pm0.031$

Table 6
$A_{\cos\phi_h}^{UU}$ 3d asymmetries for positive and negative hadrons in the second x bin ($0.012 < x < 0.020$).

z range	p_T^h range (GeV/c)	$\langle x \rangle$	$\langle Q^2 \rangle$ (GeV/c)^2	$\langle z \rangle$	$\langle p_T^h \rangle$ (GeV/c)	$A_{\cos\phi_h}^{UU}$ (h^+)	$A_{\cos\phi_h}^{UU}$ (h^-)
0.20–0.25	0.10–0.30	0.016	1.80	0.22	0.21	$-0.014 \pm 0.008 \pm 0.008$	$-0.017 \pm 0.008 \pm 0.008$
	0.30–0.50	0.016	1.80	0.22	0.40	$-0.021 \pm 0.007 \pm 0.007$	$0.005 \pm 0.007 \pm 0.007$
	0.50–0.64	0.016	1.81	0.22	0.56	$-0.067 \pm 0.010 \pm 0.010$	$-0.044 \pm 0.010 \pm 0.010$
	0.64–1.00	0.016	1.87	0.22	0.77	$-0.039 \pm 0.010 \pm 0.010$	$-0.061 \pm 0.010 \pm 0.010$
0.25–0.32	0.10–0.30	0.016	1.80	0.28	0.21	$-0.012 \pm 0.008 \pm 0.008$	$0.005 \pm 0.009 \pm 0.009$
	0.30–0.50	0.016	1.79	0.28	0.40	$-0.013 \pm 0.007 \pm 0.007$	$-0.010 \pm 0.008 \pm 0.008$
	0.50–0.64	0.016	1.79	0.28	0.57	$-0.052 \pm 0.010 \pm 0.010$	$-0.032 \pm 0.011 \pm 0.011$
	0.64–1.00	0.016	1.84	0.28	0.78	$-0.074 \pm 0.010 \pm 0.010$	$-0.051 \pm 0.010 \pm 0.010$
0.32–0.40	0.10–0.30	0.016	1.78	0.36	0.21	$0.019 \pm 0.011 \pm 0.011$	$0.023 \pm 0.012 \pm 0.012$
	0.30–0.50	0.016	1.77	0.36	0.40	$0.003 \pm 0.009 \pm 0.009$	$0.011 \pm 0.010 \pm 0.010$
	0.50–0.64	0.016	1.78	0.36	0.57	$-0.019 \pm 0.012 \pm 0.012$	$-0.049 \pm 0.013 \pm 0.013$
	0.64–1.00	0.016	1.81	0.36	0.78	$-0.078 \pm 0.011 \pm 0.011$	$-0.075 \pm 0.011 \pm 0.011$
0.40–0.55	0.10–0.30	0.016	1.72	0.46	0.21	$0.004 \pm 0.011 \pm 0.011$	$0.013 \pm 0.012 \pm 0.012$
	0.30–0.50	0.016	1.75	0.46	0.40	$-0.013 \pm 0.010 \pm 0.010$	$0.003 \pm 0.010 \pm 0.010$
	0.50–0.64	0.016	1.78	0.46	0.57	$-0.068 \pm 0.013 \pm 0.013$	$-0.033 \pm 0.014 \pm 0.014$
	0.64–1.00	0.016	1.80	0.47	0.79	$-0.096 \pm 0.011 \pm 0.011$	$-0.075 \pm 0.012 \pm 0.012$
0.55–0.70	0.10–0.30	0.016	1.71	0.62	0.21	$-0.080 \pm 0.018 \pm 0.018$	$-0.069 \pm 0.019 \pm 0.019$
	0.30–0.50	0.016	1.70	0.62	0.40	$-0.129 \pm 0.015 \pm 0.015$	$-0.146 \pm 0.016 \pm 0.016$
	0.50–0.64	0.016	1.74	0.61	0.57	$-0.120 \pm 0.019 \pm 0.019$	$-0.055 \pm 0.021 \pm 0.021$
	0.64–1.00	0.016	1.79	0.62	0.79	$-0.100 \pm 0.015 \pm 0.015$	$-0.082 \pm 0.017 \pm 0.017$
0.70–0.85	0.10–0.30	0.016	1.65	0.77	0.22	$-0.238 \pm 0.023 \pm 0.023$	$-0.260 \pm 0.025 \pm 0.025$
	0.30–0.50	0.016	1.68	0.77	0.39	$-0.233 \pm 0.020 \pm 0.020$	$-0.237 \pm 0.023 \pm 0.023$
	0.50–0.64	0.016	1.73	0.76	0.57	$-0.122 \pm 0.029 \pm 0.029$	$-0.140 \pm 0.030 \pm 0.030$
	0.64–1.00	0.016	1.77	0.76	0.80	$-0.122 \pm 0.022 \pm 0.022$	$-0.006 \pm 0.026 \pm 0.026$

Table 7

$A^{UU}_{\cos\phi_h}$ 3d asymmetries for positive and negative hadrons in the third x bin ($0.020 < x < 0.038$).

z range	p^h_T range (GeV/c)	$\langle x \rangle$	$\langle Q^2 \rangle$ (GeV/c)^2	$\langle z \rangle$	$\langle p^h_T \rangle$ (GeV/c)	$A^{UU}_{\cos\phi_h}$ (h^+)	$A^{UU}_{\cos\phi_h}$ (h^-)
0.20–0.25	0.10–0.30	0.027	2.83	0.22	0.21	$-0.028\pm0.008\pm0.008$	$-0.015\pm0.009\pm0.009$
	0.30–0.50	0.027	2.84	0.22	0.40	$-0.039\pm0.007\pm0.007$	$-0.028\pm0.008\pm0.008$
	0.50–0.64	0.027	2.90	0.22	0.56	$-0.046\pm0.010\pm0.010$	$-0.048\pm0.011\pm0.011$
	0.64–1.00	0.027	3.07	0.22	0.77	$-0.079\pm0.010\pm0.010$	$-0.037\pm0.011\pm0.011$
0.25–0.32	0.10–0.30	0.027	2.81	0.28	0.21	$-0.007\pm0.009\pm0.009$	$-0.012\pm0.009\pm0.009$
	0.30–0.50	0.027	2.82	0.28	0.40	$-0.027\pm0.008\pm0.008$	$-0.017\pm0.008\pm0.008$
	0.50–0.64	0.027	2.84	0.28	0.57	$-0.053\pm0.011\pm0.011$	$-0.029\pm0.011\pm0.011$
	0.64–1.00	0.027	2.96	0.28	0.78	$-0.077\pm0.010\pm0.010$	$-0.050\pm0.011\pm0.011$
0.32–0.40	0.10–0.30	0.027	2.77	0.36	0.21	$-0.026\pm0.011\pm0.011$	$0.019\pm0.012\pm0.012$
	0.30–0.50	0.027	2.79	0.36	0.40	$-0.024\pm0.010\pm0.010$	$-0.001\pm0.010\pm0.010$
	0.50–0.64	0.027	2.85	0.36	0.57	$-0.055\pm0.013\pm0.013$	$-0.055\pm0.014\pm0.014$
	0.64–1.00	0.027	2.89	0.36	0.78	$-0.114\pm0.011\pm0.011$	$-0.084\pm0.012\pm0.012$
0.40–0.55	0.10–0.30	0.027	2.71	0.46	0.21	$-0.008\pm0.011\pm0.011$	$0.006\pm0.013\pm0.013$
	0.30–0.50	0.027	2.74	0.46	0.40	$-0.038\pm0.010\pm0.010$	$-0.026\pm0.011\pm0.011$
	0.50–0.64	0.027	2.80	0.46	0.57	$-0.066\pm0.013\pm0.013$	$-0.078\pm0.014\pm0.014$
	0.64–1.00	0.027	2.85	0.47	0.79	$-0.124\pm0.011\pm0.011$	$-0.086\pm0.011\pm0.011$
0.55–0.70	0.10–0.30	0.027	2.65	0.61	0.21	$-0.085\pm0.018\pm0.018$	$-0.072\pm0.020\pm0.020$
	0.30–0.50	0.027	2.68	0.61	0.40	$-0.110\pm0.015\pm0.015$	$-0.109\pm0.017\pm0.017$
	0.50–0.64	0.027	2.77	0.61	0.57	$-0.107\pm0.019\pm0.019$	$-0.073\pm0.022\pm0.022$
	0.64–1.00	0.027	2.82	0.62	0.79	$-0.121\pm0.015\pm0.015$	$-0.082\pm0.018\pm0.018$
0.70–0.85	0.10–0.30	0.027	2.59	0.77	0.21	$-0.176\pm0.026\pm0.026$	$-0.202\pm0.028\pm0.028$
	0.30–0.50	0.027	2.60	0.77	0.40	$-0.180\pm0.022\pm0.022$	$-0.164\pm0.025\pm0.025$
	0.50–0.64	0.027	2.68	0.77	0.57	$-0.037\pm0.029\pm0.029$	$-0.088\pm0.033\pm0.033$
	0.64–1.00	0.027	2.76	0.77	0.80	$-0.076\pm0.023\pm0.023$	$-0.029\pm0.027\pm0.027$

Table 8
$A_{\cos\phi_h}^{UU}$ 3d asymmetries for positive and negative hadrons in the last x bin ($0.038 < x < 0.130$).

z range	p_T^h range (GeV/c)	$\langle x \rangle$	$\langle Q^2 \rangle$ (GeV/c)^2	$\langle z \rangle$	$\langle p_T^h \rangle$ (GeV/c)	$A_{\cos\phi_h}^{UU}$ (h^+)	$A_{\cos\phi_h}^{UU}$ (h^-)
0.20–0.25	0.10–0.30	0.064	6.81	0.22	0.21	$-0.012 \pm 0.008 \pm 0.008$	$-0.012 \pm 0.009 \pm 0.009$
	0.30–0.50	0.064	6.87	0.22	0.40	$-0.031 \pm 0.008 \pm 0.008$	$-0.026 \pm 0.009 \pm 0.009$
	0.50–0.64	0.064	7.08	0.22	0.56	$-0.060 \pm 0.011 \pm 0.011$	$-0.022 \pm 0.013 \pm 0.013$
	0.64–1.00	0.064	7.56	0.22	0.77	$-0.065 \pm 0.012 \pm 0.012$	$-0.057 \pm 0.012 \pm 0.012$
0.25–0.32	0.10–0.30	0.064	6.75	0.28	0.21	$-0.036 \pm 0.009 \pm 0.009$	$-0.026 \pm 0.010 \pm 0.010$
	0.30–0.50	0.064	6.84	0.28	0.40	$-0.037 \pm 0.008 \pm 0.008$	$-0.042 \pm 0.009 \pm 0.009$
	0.50–0.64	0.064	6.98	0.28	0.57	$-0.052 \pm 0.012 \pm 0.012$	$-0.051 \pm 0.013 \pm 0.013$
	0.64–1.00	0.064	7.33	0.28	0.77	$-0.107 \pm 0.011 \pm 0.011$	$-0.057 \pm 0.012 \pm 0.012$
0.32–0.40	0.10–0.30	0.064	6.66	0.36	0.21	$-0.035 \pm 0.011 \pm 0.011$	$-0.031 \pm 0.013 \pm 0.013$
	0.30–0.50	0.064	6.74	0.36	0.40	$-0.054 \pm 0.010 \pm 0.010$	$-0.019 \pm 0.011 \pm 0.011$
	0.50–0.64	0.064	6.90	0.36	0.57	$-0.081 \pm 0.014 \pm 0.014$	$-0.045 \pm 0.015 \pm 0.015$
	0.64–1.00	0.065	7.19	0.36	0.78	$-0.094 \pm 0.013 \pm 0.013$	$-0.084 \pm 0.014 \pm 0.014$
0.40–0.55	0.10–0.30	0.063	6.61	0.46	0.21	$-0.027 \pm 0.013 \pm 0.013$	$-0.030 \pm 0.014 \pm 0.014$
	0.30–0.50	0.063	6.58	0.46	0.40	$-0.042 \pm 0.011 \pm 0.011$	$-0.022 \pm 0.013 \pm 0.013$
	0.50–0.64	0.064	6.77	0.46	0.57	$-0.065 \pm 0.014 \pm 0.014$	$-0.071 \pm 0.016 \pm 0.016$
	0.64–1.00	0.064	7.03	0.47	0.79	$-0.120 \pm 0.012 \pm 0.012$	$-0.075 \pm 0.013 \pm 0.013$
0.55–0.70	0.10–0.30	0.063	6.38	0.61	0.21	$-0.061 \pm 0.021 \pm 0.021$	$-0.068 \pm 0.024 \pm 0.024$
	0.30–0.50	0.063	6.52	0.61	0.40	$-0.078 \pm 0.016 \pm 0.016$	$-0.070 \pm 0.020 \pm 0.020$
	0.50–0.64	0.063	6.63	0.61	0.57	$-0.116 \pm 0.021 \pm 0.021$	$-0.047 \pm 0.026 \pm 0.026$
	0.64–1.00	0.064	6.94	0.62	0.80	$-0.137 \pm 0.016 \pm 0.016$	$-0.058 \pm 0.021 \pm 0.021$
0.70–0.85	0.10–0.30	0.060	5.96	0.77	0.22	$-0.129 \pm 0.028 \pm 0.028$	$-0.115 \pm 0.037 \pm 0.037$
	0.30–0.50	0.062	6.22	0.76	0.40	$-0.085 \pm 0.026 \pm 0.026$	$-0.159 \pm 0.030 \pm 0.030$
	0.50–0.64	0.063	6.39	0.76	0.57	$-0.024 \pm 0.032 \pm 0.032$	$-0.077 \pm 0.044 \pm 0.044$
	0.64–1.00	0.063	6.66	0.76	0.80	$-0.039 \pm 0.024 \pm 0.024$	$-0.019 \pm 0.030 \pm 0.030$

Table 9
$A^{UU}_{\cos 2\phi_h}$ 3d asymmetries for positive and negative hadrons in the first x bin ($0.003 < x < 0.012$).

z range	p_T^h range (GeV/c)	$\langle x \rangle$	$\langle Q^2 \rangle$ (GeV/c)^2	$\langle z \rangle$	$\langle p_T^h \rangle$ (GeV/c)	$A^{UU}_{\cos 2\phi_h}$ (h^+)	$A^{UU}_{\cos 2\phi_h}$ (h^-)
0.20–0.25	0.10–0.30	0.009	1.41	0.22	0.21	$0.039 \pm 0.020 \pm 0.020$	$0.044 \pm 0.021 \pm 0.021$
	0.30–0.50	0.009	1.41	0.22	0.40	$0.049 \pm 0.018 \pm 0.018$	$-0.010 \pm 0.020 \pm 0.020$
	0.50–0.64	0.009	1.40	0.22	0.56	$0.013 \pm 0.026 \pm 0.026$	$0.042 \pm 0.026 \pm 0.026$
	0.64–1.00	0.009	1.42	0.22	0.78	$0.019 \pm 0.025 \pm 0.025$	$0.058 \pm 0.026 \pm 0.026$
0.25–0.32	0.10–0.30	0.009	1.41	0.28	0.21	$0.010 \pm 0.022 \pm 0.022$	$-0.005 \pm 0.024 \pm 0.024$
	0.30–0.50	0.009	1.41	0.28	0.40	$0.073 \pm 0.020 \pm 0.020$	$0.063 \pm 0.021 \pm 0.021$
	0.50–0.64	0.009	1.41	0.28	0.57	$0.018 \pm 0.028 \pm 0.028$	$0.077 \pm 0.029 \pm 0.029$
	0.64–1.00	0.009	1.41	0.28	0.78	$-0.004 \pm 0.026 \pm 0.026$	$0.024 \pm 0.026 \pm 0.026$
0.32–0.40	0.10–0.30	0.009	1.40	0.36	0.21	$-0.030 \pm 0.029 \pm 0.029$	$-0.002 \pm 0.030 \pm 0.030$
	0.30–0.50	0.009	1.40	0.36	0.40	$0.102 \pm 0.024 \pm 0.024$	$0.083 \pm 0.025 \pm 0.025$
	0.50–0.64	0.009	1.40	0.36	0.57	$-0.007 \pm 0.033 \pm 0.033$	$0.113 \pm 0.033 \pm 0.033$
	0.64–1.00	0.009	1.41	0.36	0.78	$0.043 \pm 0.029 \pm 0.029$	$0.112 \pm 0.029 \pm 0.029$
0.40–0.55	0.10–0.30	0.009	1.39	0.46	0.21	$0.053 \pm 0.031 \pm 0.031$	$0.142 \pm 0.031 \pm 0.031$
	0.30–0.50	0.009	1.40	0.46	0.40	$0.188 \pm 0.025 \pm 0.025$	$0.174 \pm 0.026 \pm 0.026$
	0.50–0.64	0.009	1.41	0.46	0.57	$0.025 \pm 0.034 \pm 0.034$	$0.071 \pm 0.035 \pm 0.035$
	0.64–1.00	0.009	1.41	0.47	0.79	$0.019 \pm 0.029 \pm 0.029$	$0.039 \pm 0.030 \pm 0.030$
0.55–0.70	0.10–0.30	0.009	1.36	0.61	0.22	$0.225 \pm 0.047 \pm 0.047$	$0.213 \pm 0.047 \pm 0.047$
	0.30–0.50	0.009	1.38	0.62	0.40	$0.238 \pm 0.039 \pm 0.039$	$0.328 \pm 0.038 \pm 0.038$
	0.50–0.64	0.009	1.39	0.61	0.57	$0.132 \pm 0.052 \pm 0.052$	$0.105 \pm 0.056 \pm 0.056$
	0.64–1.00	0.009	1.41	0.62	0.80	$-0.134 \pm 0.044 \pm 0.044$	$0.108 \pm 0.043 \pm 0.043$
0.70–0.85	0.10–0.30	0.009	1.35	0.77	0.22	$0.174 \pm 0.067 \pm 0.067$	$0.167 \pm 0.070 \pm 0.070$
	0.30–0.50	0.009	1.37	0.77	0.39	$0.098 \pm 0.061 \pm 0.061$	$0.170 \pm 0.056 \pm 0.056$
	0.50–0.64	0.009	1.38	0.77	0.57	$0.021 \pm 0.082 \pm 0.082$	$0.075 \pm 0.088 \pm 0.088$
	0.64–1.00	0.009	1.39	0.77	0.80	$-0.182 \pm 0.066 \pm 0.066$	$-0.021 \pm 0.067 \pm 0.067$

Table 10

$A_{\cos 2\phi_h}^{UU}$ 3d asymmetries for positive and negative hadrons in the second x bin ($0.012 < x < 0.020$).

z range	p_T^h range (GeV/c)	$\langle x \rangle$	$\langle Q^2 \rangle$ (GeV/c)^2	$\langle z \rangle$	$\langle p_T^h \rangle$ (GeV/c)	$A_{\cos 2\phi_h}^{UU}$ (h^+)	$A_{\cos 2\phi_h}^{UU}$ (h^-)
0.20–0.25	0.10–0.30	0.016	1.80	0.22	0.21	$0.009 \pm 0.015 \pm 0.015$	$-0.013 \pm 0.016 \pm 0.016$
	0.30–0.50	0.016	1.80	0.22	0.40	$-0.003 \pm 0.014 \pm 0.014$	$0.037 \pm 0.015 \pm 0.015$
	0.50–0.64	0.016	1.81	0.22	0.56	$0.007 \pm 0.020 \pm 0.020$	$0.009 \pm 0.021 \pm 0.021$
	0.64–1.00	0.016	1.87	0.22	0.77	$0.025 \pm 0.020 \pm 0.020$	$-0.014 \pm 0.021 \pm 0.021$
0.25–0.32	0.10–0.30	0.016	1.80	0.28	0.21	$0.002 \pm 0.017 \pm 0.017$	$0.026 \pm 0.018 \pm 0.018$
	0.30–0.50	0.016	1.79	0.28	0.40	$0.013 \pm 0.015 \pm 0.015$	$0.000 \pm 0.016 \pm 0.016$
	0.50–0.64	0.016	1.79	0.28	0.57	$0.002 \pm 0.021 \pm 0.021$	$0.005 \pm 0.022 \pm 0.022$
	0.64–1.00	0.016	1.84	0.28	0.78	$0.057 \pm 0.020 \pm 0.020$	$0.059 \pm 0.021 \pm 0.021$
0.32–0.40	0.10–0.30	0.016	1.78	0.36	0.21	$0.056 \pm 0.021 \pm 0.021$	$0.079 \pm 0.023 \pm 0.023$
	0.30–0.50	0.016	1.77	0.36	0.40	$0.054 \pm 0.018 \pm 0.018$	$0.101 \pm 0.020 \pm 0.020$
	0.50–0.64	0.016	1.78	0.36	0.57	$0.028 \pm 0.024 \pm 0.024$	$0.012 \pm 0.028 \pm 0.028$
	0.64–1.00	0.016	1.81	0.36	0.78	$0.025 \pm 0.022 \pm 0.022$	$0.044 \pm 0.024 \pm 0.024$
0.40–0.55	0.10–0.30	0.016	1.72	0.46	0.21	$0.050 \pm 0.022 \pm 0.022$	$0.058 \pm 0.025 \pm 0.025$
	0.30–0.50	0.016	1.75	0.46	0.40	$0.090 \pm 0.019 \pm 0.019$	$0.143 \pm 0.020 \pm 0.020$
	0.50–0.64	0.016	1.78	0.46	0.57	$0.059 \pm 0.026 \pm 0.026$	$0.091 \pm 0.027 \pm 0.027$
	0.64–1.00	0.016	1.80	0.47	0.79	$0.008 \pm 0.022 \pm 0.022$	$0.078 \pm 0.023 \pm 0.023$
0.55–0.70	0.10–0.30	0.016	1.71	0.62	0.21	$0.117 \pm 0.035 \pm 0.035$	$0.132 \pm 0.036 \pm 0.036$
	0.30–0.50	0.016	1.70	0.62	0.40	$0.158 \pm 0.029 \pm 0.029$	$0.200 \pm 0.030 \pm 0.030$
	0.50–0.64	0.016	1.74	0.61	0.57	$0.174 \pm 0.037 \pm 0.037$	$0.064 \pm 0.043 \pm 0.043$
	0.64–1.00	0.016	1.79	0.62	0.79	$-0.078 \pm 0.032 \pm 0.032$	$0.052 \pm 0.034 \pm 0.034$
0.70–0.85	0.10–0.30	0.016	1.65	0.77	0.22	$0.138 \pm 0.048 \pm 0.048$	$0.143 \pm 0.051 \pm 0.051$
	0.30–0.50	0.016	1.68	0.77	0.39	$0.113 \pm 0.041 \pm 0.041$	$0.155 \pm 0.045 \pm 0.045$
	0.50–0.64	0.016	1.73	0.76	0.57	$-0.113 \pm 0.057 \pm 0.057$	$-0.100 \pm 0.071 \pm 0.071$
	0.64–1.00	0.016	1.77	0.76	0.80	$-0.174 \pm 0.049 \pm 0.049$	$0.020 \pm 0.054 \pm 0.054$

Table 11
$A_{\cos 2\phi_h}^{UU}$ 3d asymmetries for positive and negative hadrons in the third x bin ($0.020 < x < 0.038$).

z range	p_T^h range (GeV/c)	$\langle x \rangle$	$\langle Q^2 \rangle$ (GeV/c)^2	$\langle z \rangle$	$\langle p_T^h \rangle$ (GeV/c)	$A_{\cos 2\phi_h}^{UU}$ (h^+)	$A_{\cos 2\phi_h}^{UU}$ (h^-)
0.20–0.25	0.10–0.30	0.027	2.83	0.22	0.21	$-0.020\pm0.016\pm0.016$	$-0.030\pm0.018\pm0.018$
	0.30–0.50	0.027	2.84	0.22	0.40	$-0.003\pm0.014\pm0.014$	$0.029\pm0.015\pm0.015$
	0.50–0.64	0.027	2.90	0.22	0.56	$0.003\pm0.021\pm0.021$	$0.038\pm0.023\pm0.023$
	0.64–1.00	0.027	3.07	0.22	0.77	$0.011\pm0.022\pm0.022$	$0.064\pm0.023\pm0.023$
0.25–0.32	0.10–0.30	0.027	2.81	0.28	0.21	$0.032\pm0.017\pm0.017$	$0.028\pm0.018\pm0.018$
	0.30–0.50	0.027	2.82	0.28	0.40	$0.028\pm0.015\pm0.015$	$0.020\pm0.017\pm0.017$
	0.50–0.64	0.027	2.84	0.28	0.57	$-0.005\pm0.022\pm0.022$	$0.058\pm0.024\pm0.024$
	0.64–1.00	0.027	2.96	0.28	0.78	$0.019\pm0.021\pm0.021$	$0.052\pm0.022\pm0.022$
0.32–0.40	0.10–0.30	0.027	2.77	0.36	0.21	$0.014\pm0.022\pm0.022$	$0.091\pm0.023\pm0.023$
	0.30–0.50	0.027	2.79	0.36	0.40	$0.045\pm0.019\pm0.019$	$0.050\pm0.021\pm0.021$
	0.50–0.64	0.027	2.85	0.36	0.57	$0.016\pm0.026\pm0.026$	$0.059\pm0.027\pm0.027$
	0.64–1.00	0.027	2.89	0.36	0.78	$0.040\pm0.023\pm0.023$	$0.075\pm0.025\pm0.025$
0.40–0.55	0.10–0.30	0.027	2.71	0.46	0.21	$0.070\pm0.022\pm0.022$	$0.066\pm0.025\pm0.025$
	0.30–0.50	0.027	2.74	0.46	0.40	$0.051\pm0.019\pm0.019$	$0.082\pm0.022\pm0.022$
	0.50–0.64	0.027	2.80	0.46	0.57	$0.097\pm0.025\pm0.025$	$0.077\pm0.028\pm0.028$
	0.64–1.00	0.027	2.85	0.47	0.79	$-0.014\pm0.022\pm0.022$	$0.020\pm0.023\pm0.023$
0.55–0.70	0.10–0.30	0.027	2.65	0.61	0.21	$0.090\pm0.037\pm0.037$	$0.093\pm0.040\pm0.040$
	0.30–0.50	0.027	2.68	0.61	0.40	$0.090\pm0.029\pm0.029$	$0.129\pm0.032\pm0.032$
	0.50–0.64	0.027	2.77	0.61	0.57	$0.008\pm0.037\pm0.037$	$0.072\pm0.044\pm0.044$
	0.64–1.00	0.027	2.82	0.62	0.79	$-0.013\pm0.032\pm0.032$	$0.017\pm0.038\pm0.038$
0.70–0.85	0.10–0.30	0.027	2.59	0.77	0.21	$0.160\pm0.048\pm0.048$	$0.070\pm0.054\pm0.054$
	0.30–0.50	0.027	2.60	0.77	0.40	$0.074\pm0.044\pm0.044$	$0.052\pm0.053\pm0.053$
	0.50–0.64	0.027	2.68	0.77	0.57	$-0.038\pm0.056\pm0.056$	$0.003\pm0.069\pm0.069$
	0.64–1.00	0.027	2.76	0.77	0.80	$-0.077\pm0.048\pm0.048$	$-0.120\pm0.057\pm0.057$

Table 12
$A_{\cos\phi_h}^{UU}$ 3d asymmetries for positive and negative hadrons in the last x bin ($0.038 < x < 0.130$).

z range	p_T^h range (GeV/c)	$\langle x \rangle$	$\langle Q^2 \rangle$ (GeV/c)^2	$\langle z \rangle$	$\langle p_T^h \rangle$ (GeV/c)	$A_{\cos 2\phi_h}^{UU}$ (h^+)	$A_{\cos 2\phi_h}^{UU}$ (h^-)
0.20–0.25	0.10–0.30	0.064	6.81	0.22	0.21	$-0.008 \pm 0.017 \pm 0.017$	$0.001 \pm 0.018 \pm 0.018$
	0.30–0.50	0.064	6.87	0.22	0.40	$0.010 \pm 0.016 \pm 0.016$	$0.003 \pm 0.018 \pm 0.018$
	0.50–0.64	0.064	7.08	0.22	0.56	$0.014 \pm 0.023 \pm 0.023$	$0.026 \pm 0.026 \pm 0.026$
	0.64–1.00	0.064	7.56	0.22	0.77	$0.074 \pm 0.025 \pm 0.025$	$0.041 \pm 0.026 \pm 0.026$
0.25–0.32	0.10–0.30	0.064	6.75	0.28	0.21	$-0.004 \pm 0.019 \pm 0.019$	$-0.004 \pm 0.021 \pm 0.021$
	0.30–0.50	0.064	6.84	0.28	0.40	$-0.021 \pm 0.017 \pm 0.017$	$-0.002 \pm 0.019 \pm 0.019$
	0.50–0.64	0.064	6.98	0.28	0.57	$-0.005 \pm 0.024 \pm 0.024$	$-0.043 \pm 0.026 \pm 0.026$
	0.64–1.00	0.064	7.33	0.28	0.77	$0.021 \pm 0.023 \pm 0.023$	$0.085 \pm 0.024 \pm 0.024$
0.32–0.40	0.10–0.30	0.064	6.66	0.36	0.21	$-0.007 \pm 0.024 \pm 0.024$	$0.003 \pm 0.026 \pm 0.026$
	0.30–0.50	0.064	6.74	0.36	0.40	$-0.003 \pm 0.020 \pm 0.020$	$0.036 \pm 0.023 \pm 0.023$
	0.50–0.64	0.064	6.90	0.36	0.57	$0.016 \pm 0.028 \pm 0.028$	$0.064 \pm 0.029 \pm 0.029$
	0.64–1.00	0.065	7.19	0.36	0.78	$0.061 \pm 0.025 \pm 0.025$	$0.036 \pm 0.028 \pm 0.028$
0.40–0.55	0.10–0.30	0.063	6.61	0.46	0.21	$0.052 \pm 0.025 \pm 0.025$	$0.029 \pm 0.030 \pm 0.030$
	0.30–0.50	0.063	6.58	0.46	0.40	$0.047 \pm 0.021 \pm 0.021$	$0.038 \pm 0.025 \pm 0.025$
	0.50–0.64	0.064	6.77	0.46	0.57	$-0.034 \pm 0.029 \pm 0.029$	$0.063 \pm 0.033 \pm 0.033$
	0.64–1.00	0.064	7.03	0.47	0.79	$0.018 \pm 0.023 \pm 0.023$	$0.091 \pm 0.026 \pm 0.026$
0.55–0.70	0.10–0.30	0.063	6.38	0.61	0.21	$0.101 \pm 0.040 \pm 0.040$	$-0.002 \pm 0.048 \pm 0.048$
	0.30–0.50	0.063	6.52	0.61	0.40	$-0.025 \pm 0.033 \pm 0.033$	$0.018 \pm 0.041 \pm 0.041$
	0.50–0.64	0.063	6.63	0.61	0.57	$0.046 \pm 0.041 \pm 0.041$	$0.033 \pm 0.051 \pm 0.051$
	0.64–1.00	0.064	6.94	0.62	0.80	$-0.087 \pm 0.034 \pm 0.034$	$0.027 \pm 0.043 \pm 0.043$
0.70–0.85	0.10–0.30	0.060	5.96	0.77	0.22	$-0.060 \pm 0.064 \pm 0.064$	$-0.074 \pm 0.081 \pm 0.081$
	0.30–0.50	0.062	6.22	0.76	0.40	$-0.004 \pm 0.051 \pm 0.051$	$0.043 \pm 0.065 \pm 0.065$
	0.50–0.64	0.063	6.39	0.76	0.57	$-0.043 \pm 0.063 \pm 0.063$	$0.002 \pm 0.088 \pm 0.088$
	0.64–1.00	0.063	6.66	0.76	0.80	$-0.068 \pm 0.050 \pm 0.050$	$-0.062 \pm 0.065 \pm 0.065$

Acknowledgements

References

[1] R. Feynman, Caltech lectures, spring 1972, in: Photon–Hadron Interactions, Addison–Wesley, 1998. Reprinted in Advanced Book Classics.
[2] F. Ravndal, Phys. Lett. B 43 (1973) 301.
[3] H. Georgi, H.D. Politzer, Phys. Rev. Lett. 40 (1978) 3.
[4] R.N. Cahn, Phys. Lett. B 78 (1978) 269.
[5] J.J. Aubert, et al., European Muon Collaboration, Phys. Lett. B 130 (1983) 118.
[6] M. Arneodo, et al., European Muon Collaboration, Z. Phys. C 34 (1987) 277.
[7] M.R. Adams, et al., E665 Collaboration, Phys. Rev. D 48 (1993) 5057.
[8] J. Breitweg, et al., ZEUS Collaboration, Phys. Lett. B 481 (2000) 199.
[9] V. Barone, et al., Phys. Rev. D 78 (2008) 045022.
[10] For recent reviews see V. Barone, et al., Prog. Part. Nucl. Phys. 65 (2010) 267;
     C.A. Aidala, et al., Rev. Mod. Phys. 85 (2013) 655.
[11] J.C. Collins, Foundations of Perturbative QCD, Cambridge University Press, London, 2011.
[12] A. Airapetian, et al., HERMES Collaboration, Phys. Rev. Lett. 103 (2009) 152002.
[13] C. Adolph, et al., COMPASS Collaboration, Phys. Lett. B 717 (2012) 383.
[14] D. Boer, P.J. Mulders, Phys. Rev. D 57 (1998) 5780.
[15] A. Airapetian, et al., HERMES Collaboration, Phys. Rev. D 87 (2013) 012010.
[16] M. Osipenko, et al., CLAS Collaboration, Phys. Rev. D 80 (2009) 032004.
[17] A. Bacchetta, et al., J. High Energy Phys. 0702 (2007) 093.
[18] W. Käfer, COMPASS Collaboration, in: Proceedings of Transversity 2008, Ferrara, Italy, May 2008, pp. 28–31, arXiv:0808.0114 [hep-ex].
[19] E.S. Ageev, et al., COMPASS Collaboration, Nucl. Phys. B 765 (2007) 31.
[20] P. Abbon, et al., COMPASS Collaboration, Nucl. Instrum. Methods A 577 (2007) 455.
[21] M. Alekseev, et al., COMPASS Collaboration, Phys. Lett. B 673 (2009) 127.
[22] G. Ingelman, A. Edin, J. Rathsman, Comput. Phys. Commun. 101 (1997) 108.
[23] GEANT – detector description and simulation tool, http://wwwasdoc.web.cern.ch/wwwasdoc/geant_html3/geantall.html.
[24] CORAL, The COMPASS Reconstruction Program, http://coral.web.cern.ch/coral/.
[25] C. Adolph, et al., COMPASS Collaboration, Phys. Lett. B 718 (2013) 922.
[26] H.L. Lai, et al., CTEQ Collaboration, Eur. Phys. J. C 12 (2000) 375, http://users.phys.psu.edu/~cteq/CTEQ5Table/.
[27] I. Akushevich, et al., RADGEN 1.0, arXiv:hep-ph/9906408, 1999.
[28] A. Afanasev, private communications.
[29] H. Avakian, et al., CLAS Collaboration, Phys. Rev. D 69 (2004) 112004.
[30] A. Airapetian, et al., HERMES Collaboration, Phys. Lett. B 648 (2007) 164.
[31] M. Boglione, et al., Phys. Rev. D 84 (2011) 034033.
[32] V. Barone, et al., Phys. Rev. D 81 (2010) 114026.